Molecular Therapy
Nucleic Acids
Original Article

Targeted allele-specific *FGFR2* knockdown *via* human recombinant ferritin nanoparticles for personalized treatment of Crouzon syndrome

Federica Tiberio,[1,2] Martina Salvati,[1] Luca Polito,[1] Giada Tisci,[3,6] Alessia Vita,[1] Ornella Parolini,[1,2] Luca Massimi,[4,5] Lorena Di Pietro,[1,2] Pierpaolo Ceci,[6] Gianpiero Tamburrini,[4,5] Alessandro Arcovito,[7] Elisabetta Falvo,[6,8] and Wanda Lattanzi[1,4,8]

[1]Dipartimento Scienze della Vita e Sanità Pubblica, Università Cattolica del Sacro Cuore, Largo Francesco Vito 1, 00168 Rome, Italy; [2]Fondazione Policlinico Universitario A. Gemelli IRCCS, Largo Agostino Gemelli 1, 00168 Rome, Italy; [3]Department of Biochemical Sciences, Sapienza University of Rome, P.le Aldo Moro 5, 00185 Rome, Italy; [4]Unità Operativa Complessa di Neurochirurgia Infantile, Fondazione Policlinico Universitario A. Gemelli IRCCS, Largo Agostino Gemelli 1, 00168 Rome, Italy; [5]Dipartimento di Neuroscienze, Università Cattolica del Sacro Cuore, Largo Francesco Vito 1, 00168 Rome, Italy; [6]CNR-National Research Council of Italy, Institute of Molecular Biology and Pathology, P.le Aldo Moro 7, 00185 Rome, Italy; [7]Dipartimento di Scienze Biotecnologiche di Base, Cliniche Intensivologiche e Perioperatorie, Università Cattolica del Sacro Cuore, Largo Francesco Vito 1, 00168 Rome, Italy

Crouzon syndrome is a rare genetic craniofacial malformation caused by heterozygous gain-of-function mutations in the *FGFR2* gene. The resulting constitutive activation of the FGFR2 signaling causes the premature osteogenic differentiation of calvarial mesenchymal stromal cells in skull sutures, leading to early suture ossification. Craniectomy is the gold standard treatment, being invasive and burdened by complications. To address these issues, we developed personalized allele-specific (AS) small interfering RNA (siRNA) to knockdown the expression of the *FGFR2* mutant allele in Crouzon patient-derived suture cells. The selected therapeutic siRNA mitigated FGFR2 cascade downregulating phosphorylation of FGFR2 (48%) and of its key effector ERK1/2 (77%) as RUNX2 protein levels (34%). This effect was confirmed by the reduced osteogenic commitment and differentiation of treated cells, evidenced by decreased expression of osteogenic marker genes and a 5-fold decrease in mineralized matrix deposition. We developed a highly biocompatible delivery system for siRNAs, based on human recombinant ferritin nanoparticles (NPs), combining cell targeting with improved nucleic acid encapsulation and endosomal escape properties. We demonstrated the ability of these NPs to deliver and release siRNAs within target cells, sustaining their inhibitory and AS effects. Here, we show that ferritin-mediated AS *FGFR2* knockdown by siRNA represents a suitable strategy to dampen FGFR2 overactivation in patients' cells.

INTRODUCTION

Crouzon syndrome (CS) (OMIM: 123500; ORPHANET: 207) is a rare genetic disorder occurring in approximately 16.5 cases per million live births, primarily characterized by craniosynostosis and midface deformities.[1,2] CS is predominantly caused by heterozygous missense mutations in the *fibroblast growth factor receptor 2* (*FGFR2*) gene, with a gain-of-function (GoF) effect and autosomal dominant inheritance.[3] *FGFR2* mutations occur d*e novo* in more than 50% of cases, causing sporadic cases to be way more frequently observed than familial recurrence.[3–8] FGFR2 is largely expressed in mesenchymal stromal cells, osteoprogenitors, and differentiating osteoblasts within cranial sutures, where it regulates their proliferation and differentiation via the activation of multiple downstream pathways, including phospholipase Cγ, extracellular-related kinase/mitogen-activated protein kinase (ERK/MAPK) and phosphatidylinositol 3-kinase as the main effectors.[9–13] The FGFR signaling cascade overactivation resulting from GoF mutations causes the accelerated osteogenic commitment of calvarial mesenchymal stromal cells (CMSCs), ultimately leading to the exhaustion of the stem cell reservoir within the suture mesenchyme and to the premature ossification of cranial sutures.[10,14,15]

CS is usually diagnosed at birth through physical examination, imaging techniques, and genetic testing.[4,16,17] Current therapeutic protocols include multiple surgeries starting with cranial vault expansion within 1 year of age, to decompress the craniostenotic skull and re-establish the intracranial pressure, hence minimizing the related complications.[18,19] Subsequent maxillofacial interventions enable reestablishing the functional and cosmetic facial anomalies.[16,20–23] Several peri-operative and/or post-operative complications frequently occur,

Received 24 July 2024; accepted 10 December 2024;
https://doi.org/10.1016/j.omtn.2024.102427.

[8]Senior author

Correspondence: Elisabetta Falvo, CNR-National Research Council of Italy, Institute of Molecular Biology and Pathology, Via degli Apuli 4, 00185 Rome, Italy.
E-mail: elisabetta.falvo@cnr.it
Correspondence: Wanda Lattanzi, Dipartimento Scienze della Vita e Sanità Pubblica, Università Cattolica del Sacro Cuore, Largo Francesco Vito 1, 00168 Rome, Italy.
E-mail: wanda.lattanzi@unicatt.it

including severe blood loss requiring massive transfusion (hence, transfusion-related adverse events) and relapse of the synostosis (i.e., resynostosis). This latter requires further repeated surgeries in up to 40% of treated patients due to the rapid postoperative bone re-growth at the site of intervention.[24–26]

The development of a noninvasive treatment to limit the progression of ongoing synostosis and/or to reduce the risk of resynostosis would provide a promising strategy able to minimize the need of multiple interventions and the associated complications, hence reducing morbidity and lethality of CS treatment.

In the last decade, several studies have already assessed the effectiveness of pharmacological strategies to inhibit the overactive FGFR signaling cascade in *in vitro* and *in vivo* models of FGFR-related syndromic craniosynostoses.[27] Given the wide pleiotropy of FGFR signaling,[28] RNA interfering approaches based on the use of small interfering RNA (siRNA) and small hairpin RNA (shRNA) offer advantages over direct FGFR targeting. Indeed, allele-specific (AS) silencing has been shown to hinder the overactive cranial suture ossification, particularly in Apert syndrome, while minimizing off-target effects.[29–31]

Additionally, researchers have been aiming to develop an efficient nanodelivery systems to overcome limitations and the challenges encountered with direct administration of naked siRNAs. Indeed, polymeric nanoparticles (NPs) have been widely exploited for the delivery of bioactive drugs and for gene transfer in gene therapy approaches for bone diseases, granting extended half-life and controlled release, and hence enhanced therapeutic effects.[32–34] In this context, human ferritin heavy chain (H-type; HFt), a naturally occurring polymeric NP serving as an iron storage molecule in cells, has been emerging as a promising drug nanodelivery system, thanks to its high biocompatibility, biodegradability, high solubility, stability, low toxicity, and low-cost production.[35–37]

Its unique cage-like structure, small size, and surface versatility make it an ideal carrier for bioactive compounds, including siRNAs.[36–40] Our group has previously demonstrated that an HFt derivative named HFt-MP-PASE is characterized by improved stability and target specificity. In this construct, HFt contains a shielding/masking polypeptide (PASE) rich in proline (P), alanine (A), serine, and glutamate (E) that is cleavable (MP sequence) in the presence of specific tumor-selective sequence (MP) proteases.[41]

In this study, we developed patient-tailored AS siRNA molecules selectively targeting the mutant allele of *FGFR2* in CMSCs derived from CS patients. The siRNAs could mitigate the overactive FGFR2 signaling cascade and re-establish the osteogenic commitment of CS patients' cells. Additionally, functionalized ferritin-based NPs have been formulated for the delivery of selected siRNAs into target cells. To achieve this, a modified version of the previously reported recombinant HFt-MP-PASE protein was developed, containing a tag of five histidine residues (HFt-HIS-PASE) to facilitate endosomal escape and the consequent release of the molecule payload in the cytoplasm.[41–44] This construct exhibited a high rate of internalization in CMSCs, delivering and releasing specific siRNAs within cell cytoplasm. Additionally, the HFt-HIS-PASE/siRNA complex optimized the biological efficiency, the safety and cell-specific targeting of the proposed gene knockdown strategy, while offering an innovative platform to be exploited for siRNA delivery.

RESULTS

The personalized AS *FGFR2*-targeting siRNA design strategy is able to selectively knockdown the mutant alleles in Crouzon patients' cells

To develop a personalized siRNA-based strategy targeting mutant *FGFR2* allele, we enrolled a cohort of pediatric patients with CS ($N = 3$) carrying three different heterozygous GoF missense pathogenic variants in the *FGFR2* gene (see Tables S1 and S2).

Each heterozygous *FGFR2* mutation identified in CS patients was used to design siRNA sequences that fully matched the mutant *FGFR2* mRNA while containing a single base difference (mismatch) with the wild-type *FGFR2* transcripts to obtain AS siRNAs. Given that the type of single nucleotide mismatch and its position along siRNA guide strand influence the functionality of siRNA molecules, we developed a set of AS siRNAs against the mutant allele of each CS patient by introducing the specific one-base mismatch at different positions, according to the literature (Figures 1A–1C).[45–47] For patient 1, the mismatch C:A was located at positions 8–12 and 14–15 from the 5′ end of siRNAs guide strand (Figure 1A), while for patient 2, the mismatch U:G was introduced at positions 10–13 and 15–16 (Figure 1B) and G:T mismatch in patient 3 was placed at positions 10–13 (Figure 1C).

Human CMSCs were efficiently isolated in primary culture from fused suture tissue fragments of CS patients to simulate a two-dimensional *in vitro* model for siRNA screening. Each set of patient-tailored siRNAs was used to treat the corresponding patient cells as to select the constructs exhibiting the highest target gene silencing coupled with mutated vs. wild-type discriminatory effect. The assay was performed using scalar siRNAs' concentration by qPCR (Figures S1–S3).

For patient 1, the siRNA designed to carry the mismatch C:A at position 11 (named si4) (Figure 1A) exhibited the most reproducible AS and inhibitory effect on the expression of the mutant *FGFR2* allele compared with controls treated with vehicle (Figure S1 and 1D). In particular, in cells treated with 1 nM of si4, the expression of the mutant *FGFR2* mRNA was reduced by more than 50%, without affecting the wild-type *FGFR2* allele expression (Figure 1D). For patient 2, we selected a pool of three siRNAs (named si8, si10, and si11) featuring a U:G mismatch at positions 10, 12, and 13, respectively (Figure 1B). The treatment with the three pooled siRNAs demonstrated an enhanced AS silencing than that obtained when using the same siRNAs individually (Figures S2 and 1E). As a result, the mutant *FGFR2* transcript was reduced by 25% in CMSC treated with 3 nM of siRNA pool, while the levels of the normal transcript remained unchanged (Figure 1E). Regarding patient 3, qPCR analysis

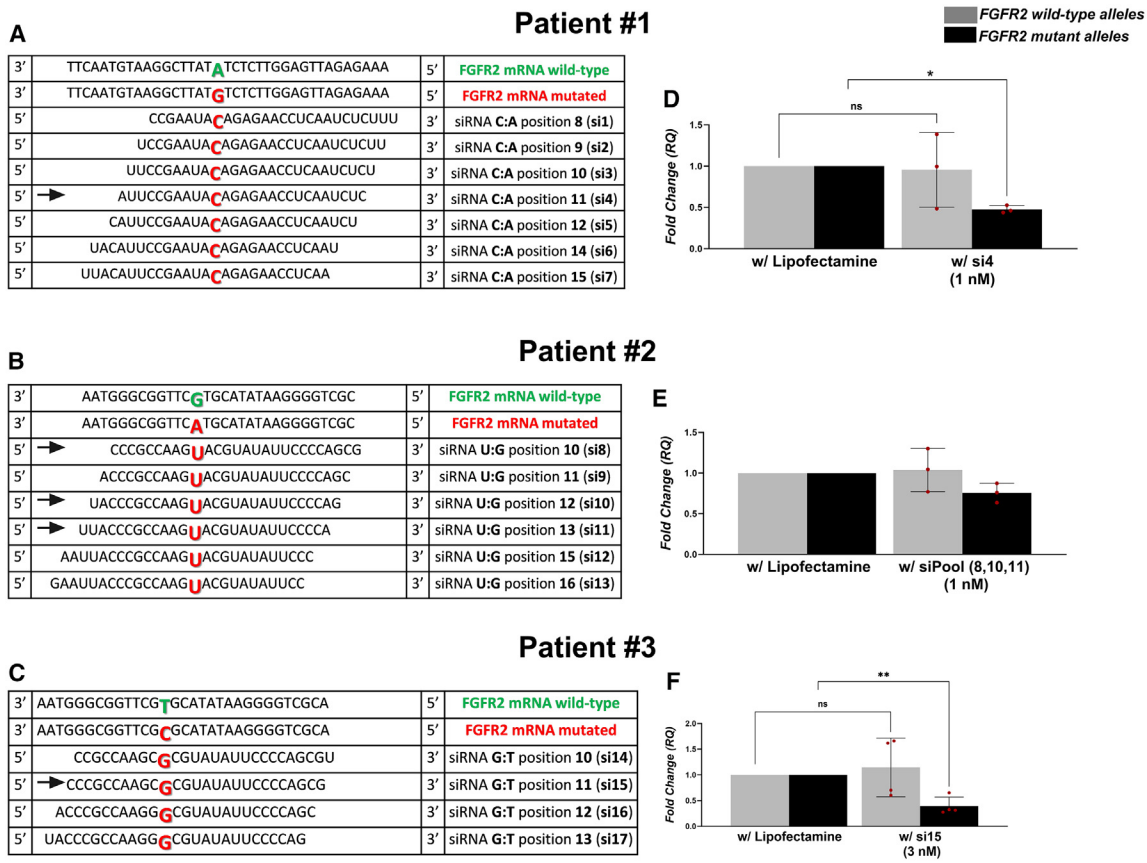

Figure 1. siRNA design and *in vitro* selection

(A–C) Tables show the sequences of siRNA designed to target three different heterozygous mutations in the *FGFR2* gene. siRNA fully matching the mutant *FGFR2* c.983A>G mRNA of CS patient 1 are reported in (A). The mismatch C:A with wild-type *FGFR2* mRNA has been introduced at positions 8–12, 14–15 from the 5′ end of siRNAs' guide strand (A). Table (B) displays siRNA sequences designed against mutant *FGFR2* transcript (c.1025G>A) of patient 2 with the mismatch located at position 10–13 and 15–16. Table (C) shows wild-type and mutant *FGFR2* transcripts (c.1024T>C) and the set of designed siRNAs with the mismatch located from position 10 to 13. (D–F) Bar graphs show wild-type (in gray) and mutant (in black) *FGFR2* expression analysis in CS patient-derived CMSCs treated with selected siRNAs for 48 h. Each siRNA was transfected into cells by cationic lipids and the effects was compared with cells treated with transfection reagent alone (with Lipofectamine). Data were normalized to *β-actin* and are expressed as fold change calculated according to $2^{-\Delta\Delta Ct}$ method. Data were analyzed using GraphPad Prism, employing Student's t test for statistical significance evaluation. *$p < 0.0119$ (D). *$p < 0.0079$ (F). ns, not significant. Results are shown as mean with error bars (SD) of at least three experiments ($n = 3$ in D and E; $n = 4$ in F).

revealed that siRNA having the G:T mismatch at position 11 (named si15) (Figure 1C) significantly inhibited the *FGFR2* mutant allele expression by 60%, while having minimal impact on the wild-type allele (Figures S3 and 1F).

Time course evaluations of the sustained effects of selected siRNA molecules revealed that silencing of the *FGFR2* mutant allele, achieved within 48 h of siRNA treatment, persisted for up to 96 h (see Figure S4). Prolonged siRNA effects at extended time points (e.g., 7 days) could not be evaluated, as cell viability was reduced due to the toxicity of the transfection reagent.

The *FGFR2* mutant AS siRNAs are capable of reprogramming Crouzon patients' cells

Functional effects of the siRNA molecule, previously developed for CS patient 1 (si4), have been investigated on FGFR2 signaling cascade. Due to the highest AS inhibitory targeting of si4 and to the limited availability of a large number of primary cultures of mutant CMSCs derived from patients, cells from patient 1 were chosen as the single use case for validation analyses. First, the silencing potency on FGFR2 expression was confirmed at the protein level by immunoblotting analysis, revealing that AS si4 downregulated total FGFR2 (t-FGFR2) protein levels by 2-fold (50%) compared with untreated cells (Figure 2). Moreover, our data demonstrated that si4 treatment reduced phospho-FGFR2 (*p*-FGFR2) levels by 48% compared with cells treated with solely Lipofectamine (Figure 2). To further investigate siRNA effects, we have analyzed changes in the protein levels of two major effectors of FGFR2-mediated signaling as ERK1/2 and Runt-2 related transcription factor (RUNX2). According to the low levels of intracellular *p*-FGFR2, siRNA-treated cells exhibited a 77% decrease in phosphorylated ERK1/2 (*p*-ERK1/2) levels, along with a 34% downregulation of RUNX2, a key regulator of osteoblast

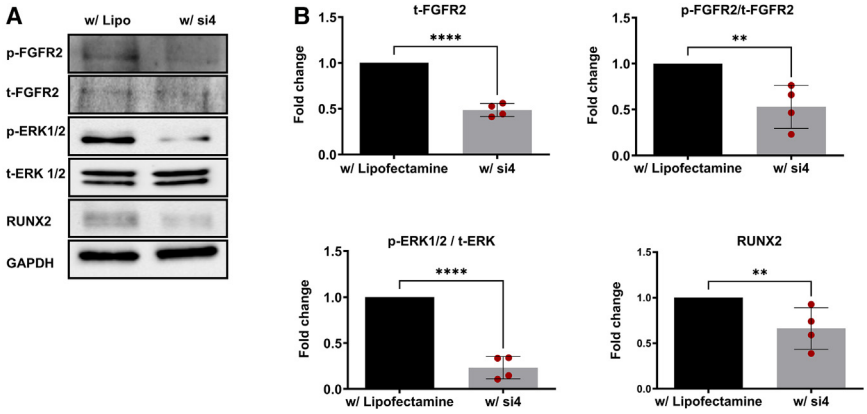

Figure 2. Effects of siRNAs on FGFR2 signaling pathway

Representative western blot images (A) and relative densitometric bar graphs (B) of total FGFR2 (t-FGFR2), *p*-FGFR2/t-FGFR2, phospho-ERK (*p*-ERK)/total-ERK (t-ERK), and RUNX2 levels in patient 1-derived CMSCs treated with 1 nM of selected siRNA (si4) for 48 h, using Lipofectamine as transfection reagent. Cells grown with only Lipofectamine were used as controls (with Lipofectamine). t-FGFR2 and RUNX2 expression levels were normalized to glyceraldehyde 3-phosphate dehydrogenase (GAPDH) and are represented as fold changes to untreated control (with Lipofectamine). All phosphorylation levels were evaluated by the ratio of phosphoprotein to total protein. The data shown are representative of four independent experiments ($n = 4$) and were analyzed by Student's t test. $^{****}p < 0.0001$; $^{**}p = 0.0071$ (*p*-FGFR2/t-FGFR2); $^{**}p = 0.0056$ (RUNX2).

differentiation, downstream the FGFR2 activation (Figure 2).[48–50] Altogether, these data confirmed the functional efficacy of si4 to mitigate FGFR2 signaling cascade overactivation.

Furthermore, to determine whether siRNA-mediated slowdown of FGFR2 signaling cascade would attenuate the osteogenic potential of FGFR2 mutation-positive osteoprogenitor cells, we cultured CMSCs under osteogenic conditions in presence of si4 (Figure 3). Our data confirmed that t-*FGFR2* mRNA levels were reduced by 61% after 5 days of osteogenic induction in si4-treated cells compared with controls treated with transfection reagent alone (with Lipofectamine) (Figure 3A). Additionally, the expression of the master bone transcription factor *RUNX2* was inhibited by 70% during osteogenic differentiation of si4-treated cells compared with the untreated cells (Figure 3A). The inhibitory effect of the selected siRNA on osteogenesis was further confirmed by the downregulation of key early stage osteogenic marker genes. Specifically, levels of *Sp7 transcription factor* (*SP7*), *alkaline phosphatase* (*ALPL*), *biomineralization associated*, *collagen type I alpha 1 chain* (*COL1A1*) and *collagen type I alpha 2 chain* (*COL1A2*) genes, were reduced by 72%, 38%, 62%, and 71%, respectively. The expression of late-stage markers including *bone gamma-carboxyglutamate protein* (*BGLAP*), and *sclerostin* (*SOST*) were also downregulated by 81% and 24%, respectively (Figure 3A). Alizarin Red (ARS) staining and quantification of the stained mineralized matrix corroborated these findings, showing a 5-fold decrease in bone matrix deposition by si4-treated cells compared with controls after 5 days of osteogenic induction (Figure 3B).

Given the recent identification of DDR2- and CTSK- expressing CMSC subpopulations in the suture niche and their involvement in premature suture fusion,[14] we evaluated the expression of these marker genes in our cellular model. This enabled assessing a higher *DDR2* versus *CSTK* transcript levels in CS patient 1-derived CMSCs (Figure 4A). Moreover, as shown in Figure 4B, we observed a reduction (15%) in *DDR2* mRNA levels in si4-treated cells compared with untreated cells (with Lipofectamine). Nevertheless, *CTSK* transcript levels were not significantly modulated compared with untreated controls (Figure 4B). Overall, these data indicated that the knockdown of mutant *FGFR2* allele in mutation-positive cells by AS siRNA may partially sustain CTSK expression marker. This defines a crucial stem cell lineage within the suture niche that is essential for proper suture ossification.[15] Additionally, this knockdown seemed to counteract *DDR2* expression, potentially mitigating the pathological expansion of the $DDR2^{+}$ subpopulation.

The functionalized HFt-HIS-PASE NPs efficiently bind selected optimized siRNA

To develop a siRNA delivery system, we designed functionalized nanovectors based on the human HFt as a promising therapeutic strategy to target CS patient cells. To this purpose, we have synthesized a modified version of the recombinant HFt, named HFt-HIS-PASE. HFt-HIS-PASE contains a tag of five histidine residues to facilitate endosomal escape (see material and methods for details).[42] HFt-HIS-PASE is shown in Figure 5A.

HFt-HIS-PASE was produced as soluble recombinant protein in *E. coli*. Typical yields were 50 mg of final pure protein per liter of bacteria culture. The purity of all the preparations was confirmed by SDS-PAGE and size-exclusion chromatography (SEC), showing the single protein band as well as the elution profile of the HFt-HIS-PASE sample (Figures 5C and 5D).

Then, we optimized si4 design using locked nucleic acid (LNA) and amino group (NH_2) modifications on siRNA sequence to improve their stability and binding to the NP surface (see description below; Figures 5A and S6). To conjugate the siRNA molecules to the HFt-HIS-PASE nanovector, we decided to use a short linker (SPDP; N-succinimidyl 3-(2-pyridyldithio)-propionate), that can be cleaved in the reducing intracellular environment for payload release.

The characterization of complex HFt-HIS-PASE/si4 by agarose gel electrophoresis demonstrated the successful binding of siRNAs on the external surface of the protein (Figures 5B and 5C). The HFt-HIS-PASE/si4 complex migrated differently as appeared significantly

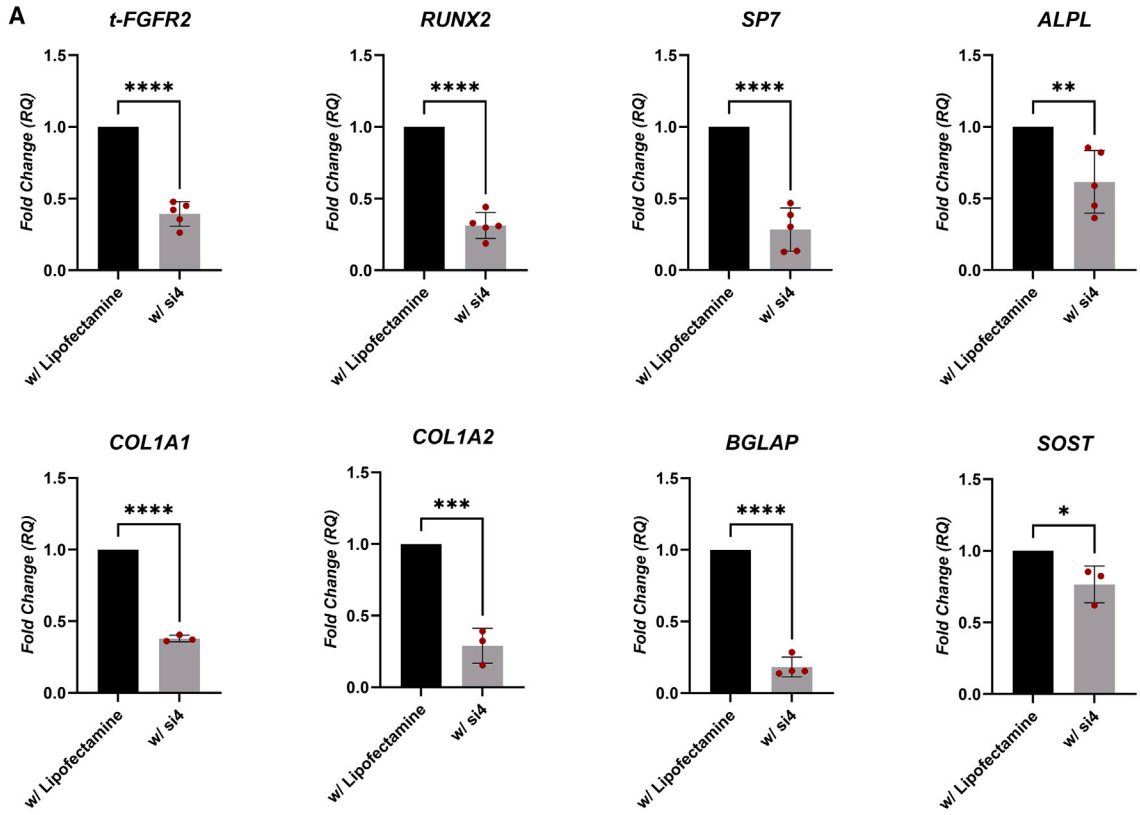

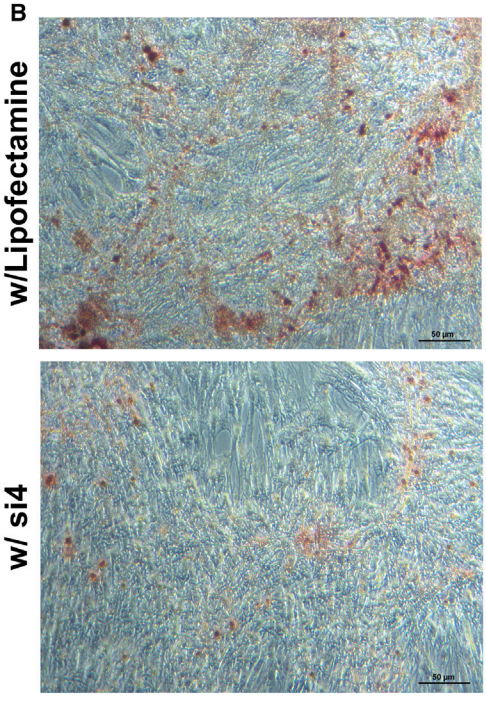

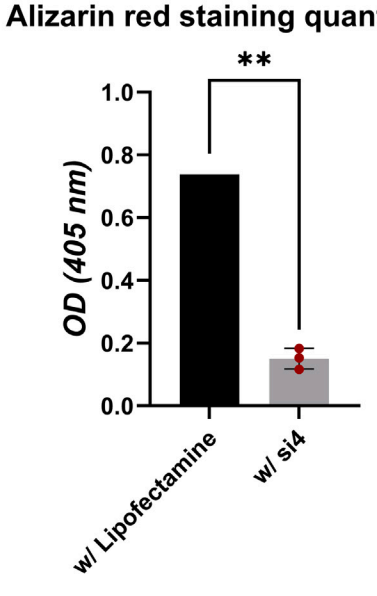

(legend on next page)

delayed compared with the naked si4 band when visualized by RNA-specific staining (Figure 5B). Additionally, the si4 molecule and HFt-HIS-PASE protein co-migrated as visualized by protein-specific staining (Figure 5C), confirming the formation of a siRNA-protein complex. To evaluate the amounts of si4 bound to the ferritin NPs, the intensities of the relative agarose bands corresponding with RNA or protein molecules were quantified using ImageJ software (https://imagej.net/ij/). Naked siRNA (NH_2-si4) or HFt-HIS-PASE molecules at a known concentration were used as reference standard. Overall, the procedure yielded a final siRNA:HFt-HIS-PASE molecular ratio of 2:1, that was approximately 10-fold higher in comparison with the canonical encapsulation approach. Purity and hydrodynamic volume of the complex HFt-HIS-PASE/si4 were determined by SEC (Figure 5D). HFt-HIS-PASE/si4 sample was found to have an elution volume and size very similar to the naked HFt-HIS-PASE protein (Figure 5D). In addition, no free siRNA was observed in the HFt-HIS-PASE/si4 sample, confirming that the siRNA molecules in solution co-eluted with the ferritin protein as a complex.

To further confirm that the modified siRNA molecules were bonded and protected from external damage, HFt-HIS-PASE/si4 sample was incubated with the enzymes RNAse or Denarase at 37°C for 1 h. No evidence of nucleic acid degradation was observed for HFt-HIS-PASE/si4 (data not shown). The absence of siRNA degradation was also assessed after three months for samples stored at 2°C–8°C. In addition, these samples stored for three months retained their silencing ability for the target gene (see below).

CMSCs express higher levels of transferrin receptor TFRC and matrix *metalloproteinases MMP-2* and *-9* during their osteogenesis

The potential application of ferritin-based NPs as siRNA delivery systems has been investigated in *in vitro* culture of CMSCs to evaluate the capability of the HFt-HIS-PASE carrier to achieve cell-specific targeting. To this purpose, we first analyzed the expression of transferrin receptor (*TFRC*) gene encoding for TFR1, which mediates the entrance of ferritin within cells (Figure 6A). Our results revealed that the expression of *TFRC* in CMSCs showed an increased expression trend during their osteogenic differentiation (Figure 6A). In fact, although *TFRC* transcript levels remained stable after 5 days of osteogenic induction, its expression was upregulated by 0.6-fold at day 10 of osteogenesis and by 3-fold at day 15 compared with undifferentiated control cells (day 0). Moreover, we have analyzed the expression of the *matrix metalloproteinases* (*MMPs*)*-2* and *-9*, as the HFt-HIS-PASE constructs include the MP motif for matrix metalloproteinase (MMP) cleavage, inserted between each HFt subunit and the outer PASE polypeptide sequence acting as a shield.[41] Despite *MMP2* mRNA levels decreased after 5 days of osteogenic induction of CMSCs, a significant increase in *MMP2* expression was observed from day 10 to day 15 (Figure 6B). In contrast, *MMP9* transcript levels remained stable during the initial 5 days of osteogenic differentiation of cells, while its expression was strongly upregulated throughout the subsequent 10-days of osteogenic induction (days 10 and 15) (Figure 6B).

HFt-HIS-PASE NPs are internalized by CMSCs and escape endosomal/lysosomal entrapment

To assess the uptake of HFt-HIS-PASE constructs in our cellular model, we analyzed and measured the internalization and intracellular trafficking of fluorescently labeled HFt-HIS-PASE (named HFt B) in CMSC cultures for 6 days, using the wild-type ferritin-based construct (named HFt A) as a control. As shown in Figure 7, both HFt constructs were efficiently internalized in CMSCs (Figure S5), with HFt B exhibiting a 2-fold increase in cellular uptake amount compared with HFt A after 15 min of incubation (Figure 7B). We observed a progressive increase in the internalization of HFt A throughout the initial 3 days of incubation (Figures 7A and 7B). Conversely, HFt B internalization kinetics was much faster: it took as little as 15 min for HFt B to reach the same levels that HFt A reached after 24 h (Figures 7A and 7B). After 3 days of incubation, both constructs exhibited comparable kinetics, indicating the attainment of a plateau phase in cellular uptake (Figures 7A and 7B). In addition, by analyzing the intracellular trafficking we noticed that both constructs were widely distributed within the CMSCs cytoplasm (Figure S5). In this regard, HFt A showed partial co-localization within lysosomal compartments after 24 h of incubation (Figure 7C), whereas HFt B fluorescence was not detectable in lysosomes (Figure 7C). Additionally, neither HFt A nor HFt B NPs were found to be distributed in the nucleus (data not shown). Overall, our data revealed that the engineered HFt B construct could be a more suitable siRNA delivery strategy, being able to enter CMSCs more rapidly than HFt A, without becoming entrapped in endo-lysosomal compartments once inside cell cytoplasm.

HFt-HIS-PASE exerts high proficiency to deliver and release therapeutic siRNA in Crouzon patient cells

The sequence of siRNA previously selected for patient 1 (si4) has been optimized by design to include LNA bases to improve its stability and functionality. In addition, a chemical modification with an amino group was introduced at the 3′ end of siRNA guide strand to allow the conjugation of si4 (NH_2-si4) on the cysteine residues present

Figure 3. Effects of siRNAs on osteogenic differentiation of CMSCs

(A) The graphs show the transcript levels of t-*FGFR2* and of the osteogenic markers such as *RUNX2*, *SP7*, *ALPL*, *COL1A1*, *COL1A2*, *BGLAP*, and *SOST* in cells treated with 1 nM of siRNA 4 (named si4) under osteogenic induction conditions for 5 days (see text for details). Cells grown with osteogenic medium supplemented with solely Lipofectamine were used as controls (w/Lipofectamine). Data were normalized to *β-actin* and are expressed as relative expression calculated according to $2^{-\Delta\Delta Ct}$ method. Results are displayed as mean ($n = 5$ in t-*FGFR2*, *RUNX2*, *SP7*, and ALPL; $n = 4$ in *BGLAP*; $n = 3$ in *COL1A1*, *COL1A2*, and *SOST*) with SD (error bars). Statistical significance was determined by Student's t test; $^{****}p < 0.0001$; $^{***}p = 0.0005$; $^{**}p = 0.0043$; $^{*}p = 0.0340$. (B) ARS staining (left images, 10×) and its quantification (right) performed in cells treated with 1 nM of si4 during osteogenic induction (5 days) and in control cells (with Lipofectamine). The graph shows ARS quantification in treated and untreated cells after 5 days of osteogenic differentiation. Graph bars represent the optical density mean values ($n = 3$) with SD. Results were analyzed by Student's t test; $^{**}p = 0.0041$.

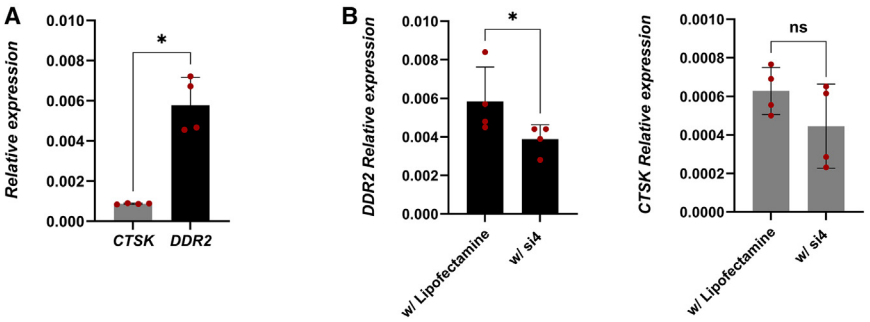

Figure 4. Cell-type-specific marker genes *DDR2* and *CTSK* expression

Bar graphs presenting differential expression of CMSC marker genes including *CTSK* and *DDR2* in CMSCs untreated (A) and treated with AS siRNA previously selected for patient 1 (named si4) (B). Data were normalized to *β-actin* and are expressed as relative expression calculated according to $2^{-\Delta\Delta Ct}$ method. Results are shown as mean (n = 4) with SD (error bars). Statistical significance was determined with Student's t test. *p = 0.0286. ns, not significant.

on the HFt-HIS-PASE surface. The ability of this naked modified siRNA (NH_2-si4) to stably silence the *FGFR2* mutant allele was confirmed in *in vitro* culture of patient 1 derived cells (Figure S6).

The final HFt-HIS-PASE/si4 complex was tested in patient 1-derived cells to assess the intracellular delivery and gene knockdown efficiency (Figure 8). Gene expression analysis demonstrated that the treatment with HFt-HIS-PASE/si4 was able to specifically knockdown the mutant *FGFR2* allele in patient 1 CMSCs compared with cells cultured with naked NPs. Specifically, upon release from the NPs into the cell cytoplasm, NH_2-si4 selectively downregulated mutant *FGFR2* mRNA levels by 65%, while the expression of the wild-type allele remained unchanged (Figure 8). By comparing the silencing effects of si4, we observed that the modified NH_2-si4 delivered by NPs had a higher AS inhibitory proficiency compared with the unmodified si4 delivered by a commercial transfection reagent (Lipofectamine) (see results above) (Figure 1).

These findings highlighted the capability of HFt-HIS-PASE NPs to efficiently deliver and release therapeutic siRNAs within cell cytoplasm, enhancing their biological effects (Figure 8).

Expected consequence and translational relevance for human pathology and therapy

The proposed HFt/siRNA combined system offers a promising adjunctive approach for addressing key surgical challenges in the

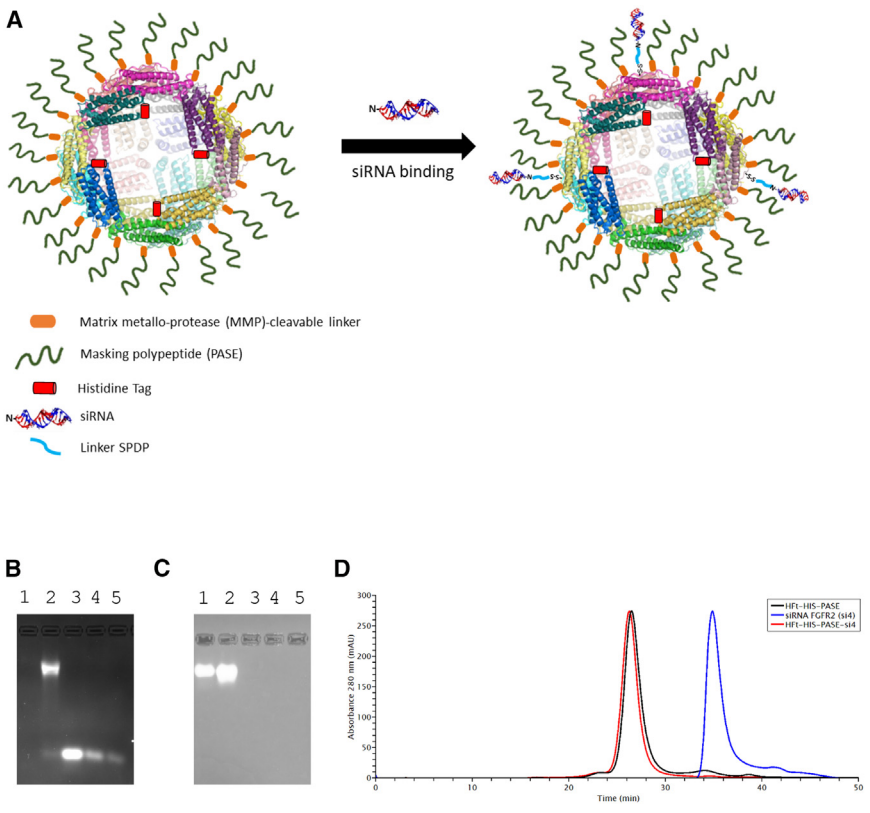

Figure 5. Development of HFt-HIS-PASE/siRNA complex

(A) Schematic representation of HFt-HIS-PASE and selected siRNA (named si4) conjugation onto NP surface. Single domains and molecules are described in the legend at the bottom of the figure. To allow the internal surface of the protein to be visualized (lighter colors), only 18 monomers out of the 24 are shown. In addition, for clarity purposes, only 4 out of the 24 histidine tags are shown. The picture has been generated with Pymol and GNU Image Manipulation Programs. (B–D) Agarose gel electrophoresis band migration profiles. Gel was double stained with Nuclei acid SYBR Gold staining for siRNAs visualization (B), and with Coomassie staining for ferritin protein visualization (C). Lane 1: HFt-HIS-PASE. Lane 2: HFt-HIS-PASE/si4 complex. Lane 3: si4 standard 2 μM. Lane 4: si4 standard 1 μM. Lane 5: si4 standard 0.5 μM. (D) size-exclusion chromatography (SEC) analysis. SEC profiles of HFt-HIS-PASE (in black), HFt-HIS-PASE/si4 complex (in red) and si4 alone (in blue).

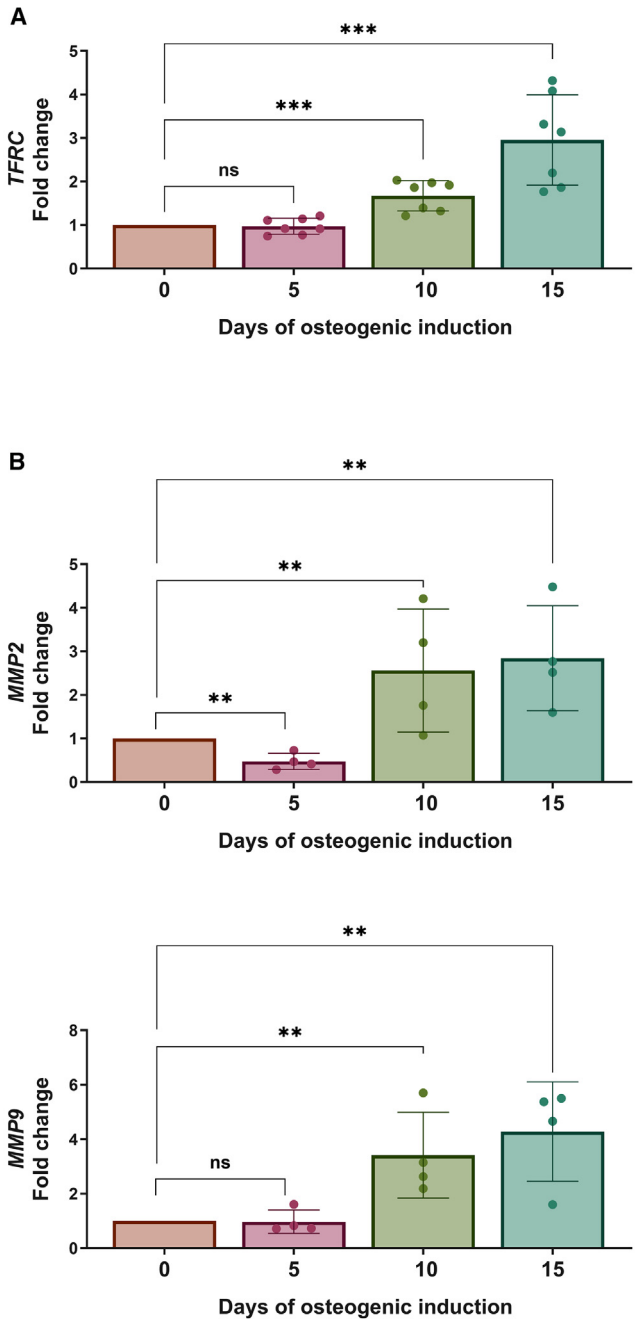

Figure 6. Expression analysis of *TFRC* and *MMP2* and *MMP9*

The histograms show the expression of *TFRC* (A) and of *matrix metalloproteinases MMP-2* and *-9* (B) during different time points of osteogenic differentiation of CMSCs (0-5-10-15 days). Results were normalized to *β-actin* and are expressed as fold change calculated according to $2^{-\Delta\Delta Ct}$ method. Data are presented as mean of $n = 7$ (A) and $n = 4$ (B) with SD (error bars). Statistical analyses were performed using Student's t test. ***$p = 0.0002$ (A). ns, not significant. **$p = 0.003$ (B-*MMP2*). **$p = 0.0079$ (B-*MMP9*).

care of CS patients. By enabling a patient-personalized, topically administered gene knockdown treatment with biocompatible, cell-targeted NPs, this strategy could potentially reduce surgical invasiveness, reoperation rates, and improve long-term outcomes.

To target CS's early cranial fusion and CMSCs, we propose applying HFt/siRNA complexes directly to affected sutures through percutaneous intra-suture injections in pre-operative and/or intra-operative settings. CS-related craniofacial abnormalities develop progressively in perinatal stages; suture ossification may complete up to 2 years after birth, with some patients showing patent sutures at birth.[51,52] In such cases, pre-operative treatment could help to delay synostosis, allowing for a more gradual surgical timeline and potentially avoiding early decompressive surgery in infants. Additionally, in cases of synostosis present at birth, intra-operative administration could prevent post-surgical resynostosis after initial craniectomy, reducing the need for repeated invasive surgeries and their associated risks, including infection, bleeding, venous air emboli, and brain damage.

We are further exploring repeated local intrasutural injections to sustain siRNA's effect, aiming for ongoing *FGFR2* allele silencing and delayed suture ossification throughout critical skull development stages.

This novel strategy, extending beyond current experimental CS therapies, seeks to improve patient outcomes in neurodevelopment, esthetics, quality of life, and social functioning. Once validated *in vivo*, this HFt-mediated siRNA approach could swiftly transition to clinical practice, as both ferritin and siRNA are already approved as generally safe for medical use. HFt is in clinical trials as a drug delivery platform (ClinicalTrials.gov: NCT05903339, NCT04645147, NCT04784767, NCT05683834).

Furthermore, recognizing that *FGFR2* GoF mutations likely drive broader phenotypic effects beyond cranial synostosis, we anticipate the potential for systemic treatment applications in the long term. Prenatal silencing of the mutated allele could offer a therapeutic window during crucial morphogenesis stages, benefiting the entire developing organism.

DISCUSSION

Currently, the mainstay of CS treatment remains surgery, with repeated transcranial procedures needed to correct the complex craniofacial deformities, involving neurosurgeons, plastic surgeons, and craniofacial surgeons. First, the neurosurgeons intervene for decompressive craniectomy, to correct the craniosynostosis, which is rapidly progressive, hence reducing the intracranial pressure and releasing the constraint on brain development.[19] Then additional maxillofacial invasive procedures are needed to correct the midfacial deformity with resulting visceral compression and associated problems.[19] Even though the adoption of complex multi-step transcranial procedures leads to better outcomes, they inevitably increase complications.[53] Each of these surgical procedures is inherently highly invasive and burdened with severe morbidity and residual lethality.

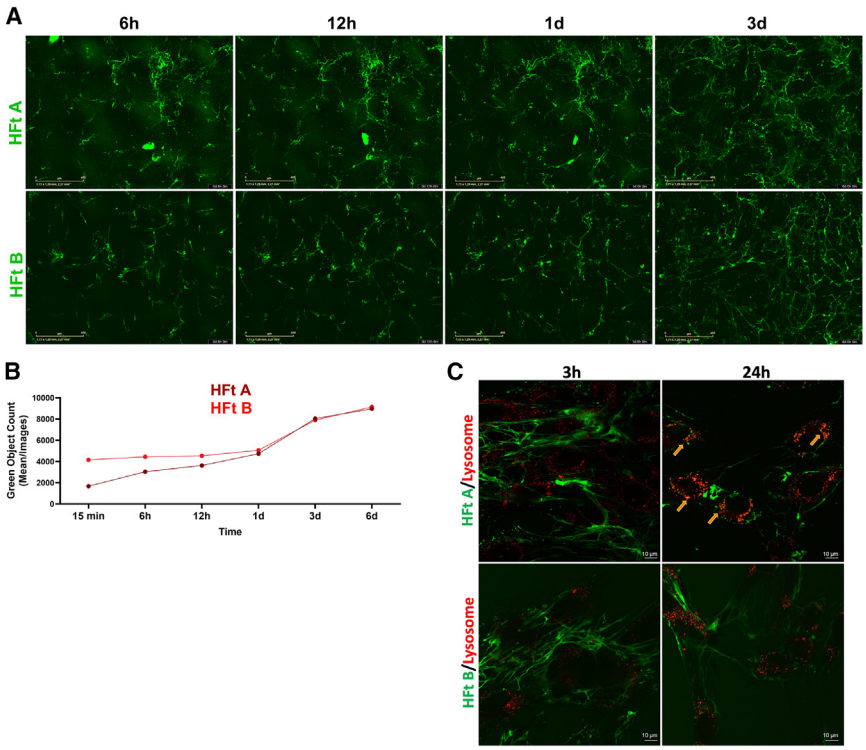

Figure 7. Analysis of cellular uptake and trafficking of HFt A and HFt B

(A) Representative images of CMSCs treated with 0.3 mg/mL of fluorescently labeled wild-type ferritin-based NPs (named HFt A) and functionalized HFt-HIS-PASE for endosomal escape (named HFt B) for 6 days by Incucyte-Live cell analysis system (10×). (B) The graph shows the quantification of green fluorescent signals detected in CMSCs treated with 0.3 mg/mL of fluorescently labeled HFt A and HFt B during different time points (15 min, 6 h, 12 h, 1 day, 3 d, and 6 d). Each condition was conducted in duplicate (n = 2) and 9 images/well have been analyzed. Data are shown as mean of green fluorescent objects detected inside cells for each condition. (C) Representative confocal microscopy images showing the biodistribution of fluorescently labeled HFt A and HFt B NPs in CMSCs after 3 and 24 h of incubation (100×). Lysosomes were stained in red using Lysotracker Deep Red.

Reoperation is seldom required, due to the high risk for relapse of synostosis (resynostosis) in syndromic cases, thus further increasing morbidities and worsening the prognosis.

In this study, we demonstrated the feasibility of a patient-customized targeted gene knockdown therapy as a noninvasive approach for CS. This therapeutic strategy was aimed to selectively silence the mutant *FGFR2* allele in CS patient cells through the design of personalized AS siRNAs, thereby restoring the proper FGFR2 signaling, preserving the pool of CMSCs subpopulation and attenuating their accelerated osteogenic commitment. Another innovative aspect of this work was the formulation of a functionalized HFt-based nanotechnology to serve as a carrier for the selected siRNA molecules, specifically targeting Crouzon patient CMSCs.

RNA interfering approaches offer advantages over direct FGFR targeting, which has been previously tested for pharmacological treatment of FGFR-related diseases. Tested approaches include inhibitors of FGFR tyrosine kinase (PD173074, PLX052, and ARQ 087) and of FGFR downstream effectors (PD98059, U0126, and SB203580), recombinant antagonist proteins as Noggin, inhibitors of heparan sulfate and antagonist of FGF ligands.[29,54–60] Functional attenuation of FGFR signaling has also been assessed through dominant-negative FGFR1 construct, domain-negative FGFR2, and soluble variants of FGFR2 receptor (sFGFG2IIIcS252W; C342Y, L424A, and R426A Fgfr2c$^{CLR/+}$).[21,55,57,61–67] Nevertheless, their translation in the clinical practice remains limited due to the nonspecific and generalized inhibition that could unpredictably affect the homeostasis of off-target cells and tissues (including limb bones, vasculature, and cell growth), also considering the wide pleiotropy of FGFR signaling.[28] Moreover, blocking antibodies against surface receptors may exert unexpected agonist effects that may worsen the disease progression.[68] Therefore, AS RNAi by avoiding or reducing the expression of the mutated receptor, would also overcome this limitation. Indeed, siRNA and/or shRNA molecules are able to target pathogenic alleles differing from the wild-type by a few nucleotides providing a promising therapeutic strategy for dominant inherited diseases caused by heterozygous mutations.[10,69] In this regard, Shukla and collaborators,[29] demonstrated the potential application of shRNA targeting the dominant mutant form of *Fgfr2* (*Fgfr2*^{S252W}) in preventing Apert-like phenotype in mice. However, a significant drawback is the constitutive transgenic expression of RNAi, which is not feasible for clinical use. Later, Luo et al.[30] showed that mutant *Fgfr2*^{P253R} allele silencing by siRNAs was able to reprogram cells isolated from Apert mice (*Fgfr2*$^{+/P253R}$). The Authors also revealed that the treatment with adeno-associated virus 9 carrying shRNA against mutant *Fgfr2* attenuated the premature closure of coronal suture and the decreased parietal bone volume in Apert syndrome mice. Recently, Myo and colleagues,[31] confirmed the effectiveness of exosome-mediated delivery of siRNA targeting *Fgfr2*^{S252W} in attenuating FGFR2 signaling cascade overactivation and thus the osteogenic differentiation of primary calvarial osteoblast-like cells isolated from calvarial sutures of Apert syndrome mice (*Fgfr2*$^{S252W/+}$). Validation of these strategies in human patient cells is still lacking, which could potentially extend the RNAi-based technology to a wider spectrum of FGFR2-related syndromic craniosynostoses, such as CS.

In this study, each enrolled CS patient carried an heterozygous GoF missense mutation in the *FGFR2* gene (c.983A>G, p.Tyr328Cys; c.1025G>A, p.Cys342Tyr; c.1024T>C, p.Cys342Arg), that has been

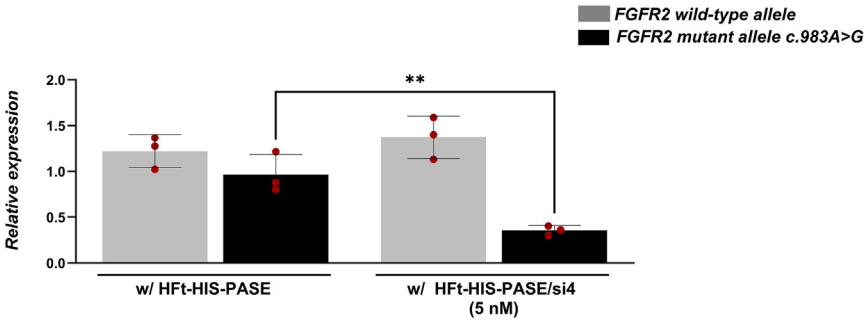

Figure 8. HFt-HIS-PASE/si4 investigation

The graph shows mutant (c.983A>G) and wild-type *FGFR2* expression levels in CMSCs derived from CS patient 1 treated with 5 nM of chemically modified siRNA 4 (NH_2-si4) delivered by HFt-HIS-PASE nanocarrier for 48 h. Cells treated with naked HFt-HIS-PASE were used as controls. Results were normalized to *β-actin* and are expressed as relative expression calculated according to $2^{-\Delta\Delta Ct}$ method. Data are presented as mean (n = 3) with SD. Data were analyzed using GraphPad Prism, employing Student's t test for statistical analysis. $^{**}p$ = 0.0096.

previously described in literature.[57,70–72] The mutation carried by CS patient 1 resulted in the replacement of amino acid tyrosine with cysteine at codon 328 (p.Tyr328Cys) in the IgIII domain of the FGFR2 protein, which is involved in the binding of FGF ligands. Indeed, the mutational spot was found highly conserved almost all tested species. On this regard, three-dimensional modeling studies have shown that the introduction of a new cysteine residue in the mutated FGFR2 protein resulted in an abnormal intermolecular cross-linking and dramatic changes in the protein structure causing severe CS phenotype.[16,73]

Instead, c.1025G>A and c.1024T>C variants identified in CS patient 2 and patient 3 confer a GoF to the mutated FGFR2 protein by the substitution of Cys342 in the IgIII domain of FGFR2, which is normally intramolecular linked to Cys278. These changes leave the Cys278 unpaired, allowing it to form intermolecular disulfide bonds. As a result, FGFR2 receptor undergoes ligand-independent dimerization, leading to the overactivation of FGFR2 signaling cascade thus accelerating the osteogenic differentiation of CMSCs.[6,73–75]

To develop siRNA molecules able to reestablish the GoF of FGFR2 signaling pathway, we designed patient-tailored AS siRNAs targeting the mutated *FGFR2* allele for each CS patient. Each siRNA sequence has been designed to perfectly match the target mutant *FGFR2* sequence while differed in one mismatched single nucleotide with the wild-type one. Given that mismatches in the region from the 3′ end to the seed sequence of siRNA provided excellent single-nucleotide discrimination, we introduced the mismatch against the wild-type allele at position from 16 to 8 away from the 5′ end of siRNA.[47] Furthermore, we developed 27-mer siRNAs, which exhibit up to a 100-fold increase in efficiency compared with conventional 21-mer.[76–78] siRNA proficiency was also achieved by placing the two-base 3′ overhang on the antisense strand and DNA residues on the blunt end of sense strand thus guiding Dicer to cleave 21–23 nucleotides upstream of the two-base overhang. The above-described design provided a more predictable and limited dicing patterns and improved the rate and efficiency of siRNA duplex entry into the RNA-inducing silencing complex.[76,77]

Among the siRNA sequences designed for each mutation, we selected a specific siRNA molecule (si4 for patient 1; si15 for patient 3) or a pool of these (si8, si10, and si11 for patient 2) that exhibited the strongest AS knocking-down effect on the expression of mutant *FGFR2* allele, without significantly influencing levels of wild-type *FGFR2* transcripts. Our results revealed that a selective gene downregulation between the perfectly matched and the single nucleotide mismatched target was achieved by placing the mismatch in the central region of the siRNA guide strand, in accordance with literature.[47,69] In addition, our results confirmed that the introduction of the mismatch after the 10th nucleotide of the siRNA guide strand, disrupting the cleavage site, preserved the annealing of wild-type allele without affecting its expression. This increased single-nucleotide discrimination proficiency.[47,69,79,80]

Further validation of our customized AS siRNA-based strategy highlighted that si4, specifically targeting the c.983A>G mutation in *FGFR2* gene, was able to mitigate FGFR2 signaling cascade overactivation as showed by the reduced levels of FGFR2 protein, of its phosphorylation and thus activation and of *p*-ERK1/2. This is a key downstream effector of FGFR2 signaling, involved in pre-osteoblast proliferation, differentiation, and calvarial suture development.[57,81,82] It has been widely described that, once activated, ERK1/2 promotes proliferation of early osteoblast precursor cells. In more mature cells, ERK1/2 enhances osteogenic differentiation contributing to the acetylation and stabilization of RUNX2, a master bone transcription factor, which drives the expression of osteogenic genes including *COL1A1*, *secreted phosphoprotein 1*, *integrin binding sialoprotein*, and *BGLAP*.[82–84] In this regard, the downstream FGFR2/MAPK signaling target, RUNX2, was downregulated in si4-treated cells, confirming the therapeutic potential of our gene knockdown approach on the entire overactive cascade.

In addition, in response to osteogenic induction, the treatment of cells with si4 decreased the expression levels of early markers of osteoblast differentiation as *RUNX2*, *SP7*, *ALPL*, *COL1A1*, *COL1A2*, and of late-stage genes including *SOST* and *BGLAP*. The efficiency of AS si4 in decelerating osteogenic differentiation has also been assessed by the reduced mineralized matrix deposited by si4-treated cells. These results validated the effectiveness of targeted knockdown of the mutant *FGFR2* to slow down the accelerated osteogenic differentiation of CS patient cells, which occurs in the cranial suture niche.

Further characterization of the effects of selected siRNAs on our cellular model revealed a reduction of *DDR2* expression in treated cells, suggesting that the mutant *FGFR2* allele silencing might restore the physiologic reservoir of CTSK$^+$ progenitors avoiding DDR2$^+$-mediated premature suture fusion.

In this regard, Bok and collaborators[14] recently displayed that CTSK$^+$ cranial suture-derived cells from a syndromic craniosynostosis patient caused craniosynostosis after xenogenic transplantation in mice. Although both the DDR2$^+$ and the CTSK$^+$ stem cell lineages contribute to the physiological calvarial suture mineralization, the authors observed a depletion of CTSK$^+$ cells followed by the expansion of DDR2$^+$ cells in affected sutures undergoing premature ossification.[14] DDR2$^+$ cells appeared to support endochondral ossification, while CTSK$^+$ promoted direct intramembranous ossification, possibly explaining the inappropriate suture ossification observed in craniosynostosis.[14] This also indicates an interaction between these two stem cell populations, which offers a novel biological interface in skull mineralization regulation as well in suture homeostasis maintenance.[14,85] Interestingly, several genes defining calvarial progenitor populations, as well as those involved in embryonic suturogenesis, are shared by DDR2$^+$ and CTSK$^+$ cell transcriptomes.[14] However, compared with CTSK$^+$, solely DDR2$^+$ cells overexpress specific craniosynostosis-related genes, including *FGFR2*.[14] This finding highlights the direct involvement of DDR2$^+$ CMSC subpopulation in the development of FGFR2-related craniosynostosis.[14,86]

The potential application of recombinant human ferritin-based NPs for siRNA delivery has been evaluated to circumvent the limitations related to the *in vitro* and *in vivo* use of naked siRNAs. These obstacles include the rapid enzymatic degradation of circulating siRNAs by RNases and the negative electrostatic charge of siRNA molecules that prevents their binding to the cell membrane and their translocation into the cytoplasm.[87–89] In this context, even though various siRNA delivery systems have been explored, including viral (e.g., adeno-associated virus) and non-viral systems (e.g., exosomes), these constructs still face limitations related to their toxicity and bioavailability, respectively. To this aim, HFt-based NPs were chosen in this study as a biomolecule carrier thanks to their high biosafety and biocompatibility, with ferritin being a natural self-constituent presents under physiological conditions both inside cells and in the bloodstream.[35] In addition, HFt-based NPs can be easily chemically or genetically modified in their surface and/or in the hollow cavity to introduce different functionalities.[35]

Another important advantage of the HFt-based system is the ability to bind to and enter cells that express TFR1 on their surface.[90] To this purpose, we demonstrated a stable expression of the *TFRC* gene encoding the TFR, in CMSCs. Interestingly, increased levels of this receptor have been observed during osteogenesis of cells, underlining that the internalization of HFt-based carrier could be favored within the prematurely ossifying sutures of Crouzon patients.

In this work, we developed a functionalized nanovector, named HFt-HIS-PASE, to be used as selected siRNA delivery system.[41] This has been formulated from a previously described HFt-MP-PASE carrier, in which the N-terminus of each HFt subunit was genetically fused to a sequence (named MP), responsive to proteolytic cleavage by metalloproteinases (MMPs) -2 and -9 followed by an outer protective polypeptide sequence (named PASE as made of a repeated proline, alanine, serine, and glutamate residues).[41] This shield was aimed at reducing the nonspecific interaction between ferritin and its receptor, allowing only in an MMP-enriched microenvironment an efficient uptake, while enhancing NP stability.[41,91] Given that CMSCs and osteoprogenitors usually release MMPs for matrix remodeling during osteogenesis, we hypothesized that the aforementioned construct could be advantageous for our delivery strategy.[92] In fact, our results confirmed that *MMP-2* and *-9* were significantly up-regulated during osteogenic induction of CMSCs, suggesting that this stimuli-responsive strategy can facilitate NP internalization in target cells committed toward osteogenic lineage, as occurs within CS skull sutures.

In this study, HFt-MP-PASE has been further engineered through a tag of five histidine residues (HFt-HIS-PASE) to achieve endosomal escape, breaking-down the organelle barriers for siRNA cytoplasmic delivery. Indeed, it is known from the literature that histidine-rich nanotransporters allowed the escape of nucleic acids from endosomes.[42,93,94]

The validation of HFt-HIS-PASE NPs as delivery nanocarrier in our cellular model corroborated the high and prompt uptake of these constructs by CMSCs. Specifically, NPs spread across the cell's cytoplasm, where successfully escaped lysosomes compartments. These results demonstrated that the natural cellular internalization of ferritin could provide a useful biological pathway to facilitate siRNA delivery within CMSC cytoplasm through receptor-mediated endocytosis, while overcoming endo-lysosomal barriers.

Once we determined that HFt-based system did not influence the functional or biological proprieties of CMSCs and was able to enter cells, we evaluated the conjugation yields of selected therapeutic siRNA onto HFt-HIS-PASE construct. In this regard, few studies demonstrated that HFt-based NPs represent a promising platform for differently charged molecules delivery, as siRNAs, protecting them from enzymatic degradation and, therefore, enhancing their stability and cell-specific targeting.[38,95] Li and collaborators[95] showed that the net surface charge of apoferritin changed from negative to positive by decreasing pH of less than 5 during the pH-dependent disassembly-reassembly method used for cargo encapsulation into HFt cavity. However, our preliminary unpublished results pointed to an unsatisfactory encapsulation yield (>0.2 siRNA molecule encapsulated per one ferritin molecule) when the nucleic acid to be encapsulated was longer than 20 base pairs. Indeed, the average size of siRNA molecules is roughly at the upper limit of the size of the apoferritin cavity that, having a diameter of 8 nm, can usually host at least one single siRNA molecule. In addition, siRNAs used in our experiments were longer than traditional 21-mer siRNAs internalized in ferritin NPs by other groups.[38,95] To this purpose, selected si4

molecules have been conjugated onto HFt-HIS-PASE surface instead of encapsulating them.

To have satisfactory stability of the complex and allow the complexation of siRNA to the NP surface, we developed LNA-[96] and NH_2-modified siRNA molecules. Specifically, LNA is highly compatible with the siRNA machinery, while improving siRNA bio-stability, inhibitory and discriminatory effects; whereas the reactive amino group NH_2 was exploited for complexation with the thiol group on HFt-HIS-PASE through the use of SPDP (N-succinimidyl 3-(2-pyridyldithio) propionate). This is a labile short linker that ensures the dissociation of the siRNA payload in the reducing intracellular environment and is characterized by a minimal steric interference in the binding between siRNA and its target. This yielded a final siRNA:HFt-HIS-PASE molecular ratio of 2:1, that was about 10-fold higher in comparison to the encapsulation approach.

The validation of the therapeutic effects of HFt-HIS-PASE/siRNA complex have shown a high efficiency of HFt-HIS-PASE NPs in siRNA delivering and releasing to target cells. In addition, the AS-silencing effect of modified si4 were preserved once these molecules were released from NPs inside cell cytoplasm. In fact, NH_2-si4 molecules maintained their stability and showed an increased silencing and discriminatory efficiency due to the chemical optimizations of the sequence design. Overall, these data highlight that HFt-HIS-PASE-based NPs represent an innovative strategy to target suture niche CMSCs through a stimuli-responsive strategy. Their efficiency as delivery systems of selected therapeutic siRNA molecules within cell cytoplasm enables the modulation of overactive FGFR2 signaling thereby correcting the aberrant osteogenic commitment of *FGFR2*-mutated cells.

In summary, this study provides the first *in vitro* proof of evidence for the development of an alternative noninvasive therapeutic approach for CS based on patient-tailored therapeutic siRNA delivered by highly biocompatible ferritin-based nanocarriers in targeted patients' cells.

Being inherently versatile, the proposed strategy might be further extended for the treatment of other rare *FGFR2*-related syndromes and genetic conditions caused by GoF heterozygous mutations in different genes.

MATERIAL AND METHODS

Patient enrollment and sample collection

The patient sample used in this study comprises three males with CS, aged 4 months to 6 years (see Tables S1 and S2), selected among a large craniosynostosis database in our institutional repository including both syndromic and non-syndromic cases. The clinical diagnosis was confirmed through Sanger sequencing analysis of the *FGFR2* gene (data not shown).

Patients were enrolled upon obtaining written informed consent from their parents. The entire study protocol was designed according to the European Good Clinical Practice guidelines and with the current revision of the Declaration of Helsinki and represents one of the projects belonging of a multicenter study on craniosynostosis approved by the Ethical Committee of the Università Cattolica del Sacro Cuore, School of Medicine (protocol IDs 19056/14 and 4876/22).

Calvarial suture tissue fragments were collected as surgical waste during the decompressive craniectomy intervention at the Pediatric Neurosurgery Unit of the Fondazione Policlinico Universitario A. Gemelli-IRCCS in Rome, Italy.

Cell isolation and culture

The tissue specimens were used for primary cell isolation, as previously described elsewhere.[97] Briefly, calvarial fragments were extensively washed in PBS (Dulbecco's PBS without calcium without magnesium, Aurogene, Rome, Italy) supplemented with 1% antibiotics (penicillin 100 IU/mL, streptomycin 100 mg/mL; Euroclone, Milan, Italy), cleaned out of any soft tissue residues and then placed into 100 mm-diameter plates. A standard growth medium (GM), represented by DMEM with high-glucose (4.5 g/L) (Aurogene), supplemented with 1% L-glutamine (Euroclone), 1% antibiotics, and 10% fetal bovine serum (FBS; Aurogene), was added and plates were then placed into a humidified incubator at 37°C and 5% CO_2. Once isolated in primary culture, cells were sub-cultivated in GM at 37°C in a 5% CO_2 atmosphere and used at passages 2–7 for subsequent analyses.

Osteogenic differentiation assay

For osteogenic differentiation assay, CMSCs were cultured with GM until confluence prior to the induction of osteogenesis. The GM was then replaced with an osteoinductive medium (OM) composed as follow: DMEM with low glucose (1 g/L) (Aurogene) supplemented with 1% L-glutamine, 1% antibiotics (penicillin 100 IU/mL, streptomycin 100 mg/mL), 10% FBS (GIBCO, ThermoFisher Scientific, Waltham, MA, USA), dexamethasone (0.1 μM), ascorbic acid (10 μM), and β-glycerophosphate (50 μM) (Sigma-Aldrich, Saint Louis, MO, USA) as previously described.[97,98] The OM was changed every 2 days during the time course experiment. Osteogenic differentiation was assessed by ARS staining (Sigma-Aldrich) and its quantification and through real-time PCR expression analysis of osteogenic markers at specified time points (see descriptions below).

ARS staining

Osteogenic differentiation was assessed using ARS staining that reacts with calcium ions, to detect *in vitro* bone mineralized matrix. The cell cultures were then morphologically examined using invertoscope (Zeiss Primovert Microscope, Oberkochen, Germany), to verify the acquisition of differentiated phenotype and the matrix mineralization at specific time points (5 days of osteogenic induction for siRNA validation, as detailed below). To quantify mineralized deposits, ARS dye was extracted from the stained monolayer by dissolving each sample in 10% acetic acid according to standardized protocol.[99] ARS adsorption spectrum at 405 nm was quantified using an automatic microplate photometer (ELx800; Biotek, Bad Friedrichshall, Germany).

Allele-specific siRNA design

The heterozygous *FGFR2* mutation found in each CS patient enrolled (see Figure 1) was used to drive the design of different siRNA sequences using *ad hoc* bioinformatic tools (Integrated DNA Technologies, IDT, Coralville, IA, USA). Each siRNA sequence has been designed and synthetized as asymmetric 27-mer RNA duplex with two-base 3′ overhang on the antisense strand, whereas the sense strand of 25 nucleotides in length presented a 3′ blunt end modified with two DNA bases.[77] Specifically, the guide strand of each siRNA fully matched the corresponding mutated *FGFR2* mRNA sequence, thus containing a single base difference (mismatch) with wild-type *FGFR2* mRNA (see Figure 1). A set of 4-to-7 siRNAs was designed for each allelic variant, introducing the mismatch at different positions from 5′ end of each siRNA guide-strand (see Figure 1), based on previous works.[47,80]

In vitro siRNA treatment

The AS silencing effect of the designed siRNAs was then evaluated in the corresponding patients' CMSCs. Specifically, siRNAs were first tested for 48 h in CMSC culture grown in standard proliferative condition (GM) to identify the most effective molecules for each allelic *FGFR2* variant-positive case. To this aim, cells were seeded at a density of 5×10^4 cells per well and grown to approximately 50%–60% confluency, then transiently transfected with siRNA using Lipofectamine RNAiMAX Transfection Reagent (Invitrogen, Carlsbad, CA, USA), according to the manufacturer's instructions. All siRNAs were tested either individually or in an equally proportioned mixed pool using scalar concentrations. Briefly, siRNA molecule(s) was diluted in culture medium (DMEM high glucose) to reach the final treatment concentration (from 0.1–10 nM), whereas 7.5 μL of Lipofectamine RNAiMAX were added in 100 μL of culture medium. To allow the formation of stable siRNA/transfectant complexes, Lipofectamine solution was incubated with the diluted siRNA(s) for 5 min at room temperature. Then, cells in GM were incubated with the resultant solution for 48 h. CMSCs treated with solely Lipofectamine were used as controls.

The long-lasting effects of siRNA were evaluated at different time points (48, 72, and 96 h) in CMSC cultures, following the protocol outlined in the transfection reagent data sheet, as described above. Subsequently, given the pre-determined and finite number of population doublings due to primary cells senescence, cells from a single use case (patient 1) were chosen for further validation of our siRNA design strategy. To this purpose, to evaluate the effect of the previously selected siRNA for patient 1 (named si4) on cell differentiation, CMSCs derived from patient 1 were treated with OM supplemented with 1 nM of si4 for 5 days. The OM was changed every 2 days, with siRNA added each time. Cells cultured in OM supplemented with Lipofectamine (without siRNA) served as positive controls for differentiation. The silencing efficiency of siRNA molecules was assessed by real-time PCR expression analysis of mutant and wild-type *FGFR2* mRNA as well as of osteogenic markers (see descriptions below).

Design of the HFt-HIS-PASE nanovector

The *HFt-HIS-PASE* gene is a variant of the *HFt-MP-PASE* gene previously reported.[41] The design of HFt-HIS-PASE protein includes, C- to N-terminus: (1) a first domain comprising the amino acid sequence of the native human ferritin HFt modified through the inclusion of five histidine residues, inserted in the external loop (referred as CD loop) of the ferritin surface; and (2) a second N-terminal domain comprising the amino acid sequence of the matrix MMP cleavage site (PLGLAG) followed by aPASE sequence (ASPAAPAPASPAEP APSAPA).

Production of HFt and HFt-HIS-PASE nanovector

The expression vector pET-27b containing the HFt gene was purchased by GENEART AG (Thermo Fisher Scientific, Waltham, MA, USA). Recombinant HFt (named HFt A) was expressed and purified from *E. coli*, as previously described.[100] The expression vectors pET-27b containing the *HFt-HIS-PASE* gene was assembled by GENEART AG (Thermo Fisher Scientific). Gene synthesis was performed taking into consideration the codon optimization for high level expression in *E. coli* BL21 (DE3) (New England BioLabs, Ipswich, MA, USA) cells harboring the recombinant gene were used for the expression of HFt-HIS-PASE protein (named HFt B). *E. coli* cells were grown first at 23°C o.n. and then at 37°C the next day to reach an optical density of 1.0 at 600 nm. Cells were grown in 1 L of terrific broth medium (Grisp, Porto, Portugal), containing kanamycin at a final concentration of 0.03 mg/mL (Serva, Heidelberg, Germany). After induction with IPTG (Isopropil-β-D-tiogalattopiranoside) 1 mM (PanReac, Monza, Italy), *E. coli* cells were incubated at 30°C for 2 h. Cells were harvested by centrifugation at 5,000 rpm for 20 min at 4°C. The recovered pellet was suspended in PBS, NaCl 150 mM and 20 mM imidazole at pH 7.4, and mixed with protease inhibitor tablets (Thermo Scientific, Rockford, IL, USA) and Phenylmethylsulfonyl fluoride 1 mM (PMSF; Thermo Scientific). Then, the DNAse enzyme (Sigma-Aldrich) was added at a final concentration of 0.1 mg/mL and cells were disrupted by sonication. Cell lysate was incubated at 37°C for 40 min and was centrifuged at 14,000 rpm for 50 min at 4°C. The supernatant was recovered and loaded in a His-Trap column (Cytiva, Uppsala, Sweden), for metal affinity chromatography, previously equilibrated with the same buffer. HFt-HIS-PASE samples were eluted with an elution buffer containing imidazole 100 mM, to separate it from *E. coli* proteins and DNA contaminants. The samples were dialyzed overnight against PBS pH 7.5, concentrated by means of 100 kDa Amicon Ultra-15 centrifugal filter devices (Millipore, Billerica, MA, USA). Finally, the HFt-HIS-PASE samples were sterile filtered and stored at 4°C (short term) or −20°C (long term).

HFt-based carriers characterization

The purity of all the HFt-based preparations was assessed by SDS-PAGE, running the samples on 15% gels and staining the proteins with Coomassie brilliant blue. Protein concentrations were determined spectrophotometrically at 280 nm using a molar extinction coefficient (on a 24-mer basis) of 4.56×10^5 M^{-1} cm^{-1} (ProtParam software, http//www.expasy.org).

SEC experiments were performed using a Superose 6 gel-filtration column equilibrated with PBS at pH 7.4. All samples were prepared at 1 mg/mL in filtered H_2O_{dd}. All the traces for SEC experiments were analyzed with QtiPlot (IONDEV SRL, Bucharest, Romania).

Fluorescent labeling of HFt-based NPs

To obtain fluorescently labeled NPs, HFt A and HFt B protein solutions (1 mg/mL) were incubated with 1 mM of Fluorescein-5-Maleimide (λ_{ex} 491 nm, λ_{em} 518 nm; Thermo Scientific) in PBS, pH 7.0 for 2 h and room temperature under stirring in the dark. Subsequently, the sample was filtered, dialyzed and exchanged with H_2O_{dd} and PBS by using 100 kDa Amicon Ultra-15 centrifugal filter devices to remove excess reagents. The samples were sterile filtered and stored at 4°C in the dark. The number of dye molecules linked per protein was determined by absorbance spectroscopy, in accordance with the manufacturer's instructions, applying the Lambert-Beer law.

AS siRNA design optimization

To produce HFt-HIS-PASE/siRNA complexes, we optimized siRNA designed for their conjugation onto NPs surface. To this aim, siRNA sequence (si4), that we have previously selected as the most efficient in patient 1 cells (see description above), has been chemically modified by introducing LNA bases and a reactive amino group at 3′ end of siRNA strand (NH_2-si4).

Modified NH_2-si4 molecule has been tested in patient 1-derived CMSCs to confirm their AS targeting effect. Briefly, cells were treated with scalar concentrations of NH_2-si4 molecule (0.1 nM, 1 nM, 10 nM) for 48 h, using Lipofectamine as transfection reagent. Real-time PCR was carried out to evaluate the expression of mutant and wild-type *FGFR2* alleles (see details below).

Formulation and characterization of HFt-HIS-PASE/siRNA complexes

The efficiency of the developed HFt-based constructs as a siRNA delivery system has been assessed by producing and testing HFt-HIS-PASE/siRNA complexes. To this aim, chemically modified si4 molecules were conjugated to HFt NPs by exploiting the complexation of the reactive amino group at 3′ end of siRNA strand (NH_2-si4; as previously described) with the thiol groups present on HFt-HIS-PASE surface through the use of the SPDP (N-succinimidyl 3-(2-pyridyldithio) propionate) cleavable crosslinker (Thermo Scientific, Rockford, IL, USA). We used a 30:1 SPDP-to-NH_2-si4 ratio in the solution that was incubated for 30 min at 20°C. To remove reaction by-products and excess nonreacted SPDP reagent, a desalting column PD MiniTrap G-25 (Cytiva), equilibrated with PBS, was used. Then about four excesses of this reactive solution was mixed with the HFt-HIS-PASE protein. The reaction mixture was incubated overnight at 20°C to allow protein-siRNA complex formation. The resulting solution was ultra-filtered at pH 7.4 and exchanged with PBS by using 100 kDa Amicon Ultra-15 centrifugal filter devices to remove unbound molecules. The HFt-HIS-PASE/si4 complex was characterized through 1.8% agarose gel electrophoresis to demonstrate the successful binding of NH_2-si4 to the protein external surface. The gel was run at 90V for 60 min and subsequently imaged using ChemiDoc (Bio-Rad, Hercules, CA, USA). The amount of si4 bound to the ferritin NPs was evaluated with the software ImageJ (https://imagej.net/ij/), enabling the calculation of the area and value statistics of pixels, in user-defined selections objects based on intensity. Standards of siRNA (as NH_2-si4) were used as reference. The gel was stained with Nucleic acid SYBR Gold staining for DNA/RNA visualization. The same analysis was used to evaluate the concentration of the protein using standards of HFt-HIS-PASE as reference after gel staining with Coomassie dye. Purity and hydrodynamic volume of the complex HFt-HIS-PASE/si4 were determined by SEC. SEC experiments were performed as already described above. Stability of HFt-HIS-PASE/si4 complex was evaluated after storage at 2°C–8°C (3 months) and in the presence of RNAse A/T1 Mix (Thermo Scientific) or Denarase (c-LEcta GmbH, Leipzig, Germany) at 12.5×10^3 U/mL. Denarase is able to cleave DNA and RNA impurities.

Analysis of *TFRC* and *MMP2* and *MMP9*

HFt-HIS-PASE complex derived from a previously reported HFt construct named HFt-MP-PASE, as detailed above. This consists of an MMP linker responsive to proteolytic cleavage by specific proteases (MMP-2 and -9) inserted between each HFt subunit and the outer masking PASE polypeptide. The PASE mask was aimed at increasing the stability of modified protein variants. The presence of PASE is also capable of masking the protein surface and thus of extending its plasma half-life and target specificity.

To evaluate the potential application of functionalized HFt-HIS-PASE constructs in our cellular model, we have investigated the expression levels of *TFRC* and of *matrix metalloproteinases-2* and *-9* to optimize the site on NPs. To this aim, CMSCs were cultured with GM to confluence prior to the induction of osteogenesis as previously described. Cells were then induced toward the osteogenic differentiation by OM (as specified in previous sections) in a time-course experiment. The expression of and of *MMP2* and *MMP9* was evaluated during different time points (0-5-10-15 days of osteogenic induction), using real-time PCR (see RNA isolation and gene expression analysis below).

Fluorescence microscopy

Cellular uptake of HFt NPs were preliminary analyzed by fluorescence microscopy (Zeiss AXIO Imager, Jena, Germany). Briefly, CMSCs were seeded at a density of 2×10^4 cells/well in glass coverslips (Sigma-Aldrich) and cultured with standard GM for 24 h. Subsequently, cells were treated with 0.5 mg/mL of fluorescently-labeled HFt constructs for different time points (5-10-30-60 min). After incubation cells were extensively washed with PBS to remove culture medium residues and then fixed with 4% paraformaldehyde (PFA) solution. After 15 min of incubation, PFA was removed and then, 6-diamidino-2-phenylindole (λex 358 nm; λem 461 nm) solution, a blue fluorescent dsDNA stain, was added to stain nuclei of fixed cells. After 5-10-30 and 60 min of treatment with HFt, cells were observed through fluorescence microscopy. NP's uptake was calculated by measuring the fluorescence intensity per cell nuclei through ImageJ software.

Cellular uptake and trafficking of HFt-NPs

To analyze the ability of the wild-type HFt and HFt-HIS-PASE (HFt A and HFt B, respectively) nanovectors to recognize CMSCs we performed the following experiment. CMSCs were seeded at a density of 2×10^4 cells/well in a 24-well plate (Corning, Corning, New York, USA) and cultured with standard GM for 24 h. Subsequently, cells were treated with 0.1 mg/mL (data not shown) and 0.3 mg/mL (see Figure 7) of fluorescently labeled HFt A and HFt B constructs and placed into Incucyte Live-Cell Analysis system incubator (Sartorius, Gottinga, Germany) for 6 days. Fluorescent signals were detected using phase contrast and green (300-ms exposure) channels in the Incucyte platform. Specifically, for each condition, nine image sets from distinct regions per well were taken every 15 min for the first 2 h and then every 4 h for 6 days using a 10× objective. The efficiency of HFt entry was evaluated by measuring the average number of green objects resulting from nine images per well at different time points. Each condition has been repeated in duplicate (n = 2). Images of untreated cells were selected as negative control for background correction. Graphics were generated with IncuCyte Basic Software graph/export functions.

Tracking of lysosomes

To investigate the difference between HFt (HFt A) and HFt-HIS-PASE (HFt B) nanovectors in escaping the endo-/lysosomal compartments, we performed the following experiment. Briefly, cells were seeded at a density of 15×10^3 in an eight-well chamber slide (Ibidi, Munich, Germany) and cultured in standard GM for 24 h. Then, cells were incubated with prewarmed (37°C) Lysotracker Deep Red (Invitrogen)-containing medium, according to manufacturer's instructions. After 2 h, the medium was replaced with fresh medium and cells were treated with 0.3 mg/mL of fluorescently-labeled HFt A and HFt B. After 3 h and 24 h of incubation, images of live cell were acquired with confocal laser scanning microscopy (Nikon A1 MP+, Nikon). The experiments were repeated in triplicate ($n = 3$).

In vitro testing of HFt-HIS-PASE/si4 constructs

The construct consisting of modified NH_2-si4 molecule selected for CS patient 1 conjugated onto HFt surface (HFt-HIS-PASE/si4) has been tested in patient 1 cells to evaluate siRNA delivery and release efficiency. To this aim, CMSCs derived from CS patient 1 were plated at a density of 5×10^4 cells/well in a 12-well plate and cultured in GM until they reached 50%–60% confluence. Then, CMSCs were treated with 5 nM of NH_2-si4 delivered by HFt-HIS-PASE NPs (HFt-HIS-PASE/si4) for 48 h. Cells treated with naked HFt-HIS-PASE were used as controls. Each experimental condition was performed in triplicate ($n = 3$). The effects of the described treatment were investigated through real-time PCR expression analysis of mutant and wild-type *FGFR2* mRNA (see method below).

RNA isolation and gene expression analysis

Real-time PCR (qPCR) was used to quantitatively analyze the expression of *β-actin* (*ACTB*), mutant and wild-type *FGFR2*, *t-FGFR2*, *TFRC*, *MMP2*, and *MMP9* as well as to quantify levels of osteogenic markers including *RUNX2*, *SP7*, *ALPL*, *COL1A1*, *COL1A2*, *BGLAP*, and *SOST* after osteogenic induction assay (Table S3).

To this purpose, total RNA was isolated from cell pellet using Reliaprep RNA Miniprep Systems (Promega, San Luis Obispo, CA, USA) in accordance with the procedures described by the manufacturer. Isolated RNA was quantified using a UV spectrophotometer (NanoDrop One/OneC Microvolume UV-Vis, Thermo Scientific). Then, up to 500 ng/μL of total RNA of each sample were reverse transcribed into cDNA using GoScript Reverse Kit (Promega) following the manufacturer's protocol. qPCR of above-mentioned genes was performed using GoTaq(R) qPCR Master Mix (Promega) and TaqMan Universal PCR Master Mix (Thermo Fisher Scientific). Specifically, sequence-specific fluorescent oligonucleotide Taqman probes and primers (Thermo Fisher Scientific) were designed to evaluate the expression levels of wild-type and mutant *FGFR2* transcripts in CS patient cells treated with siRNAs and with HFT-HIS-PASE/siRNA complexes (Table S3). TaqMan probes were formulated with a dye label (FAM or VIC) on the 5′ end, a minor groove binder and nonfluorescent quencher on the 3′ end. The relative expression of genes was obtained normalizing data to *β-actin* and results were calculated using $2^{-\Delta\Delta Ct}$ method.

Western blotting

Molecular effects of siRNA developed for CS patient 1 were determined at protein level, evaluating changes in FGFR2 expression and in MAPK signaling transduction. Following 48 h of incubation with siRNAs and solely Lipofectamine (controls), cells were mechanically harvested on ice and homogenized to proceed with protein extraction. Whole cell extracts were isolated using RIPA Lysis Buffer (20 mM Tris-HCl pH 8.0, 150 mM NaCl, 1 mM Na2-EDTA, 1 mM EGTA, 2.5 mM Na-pyrophosphate, 1% Triton X-100, 10% glycerol) (Bio-Rad) supplemented with protease and phosphatase inhibitors (Sigma-Aldrich) and with 2% beta-mercaptoethanol. The concentration of the isolated proteins was determined using BCA Protein Assay Reagent (Invitrogen). Proteins were fractionated by a gradient (4%–10%) SDS-PAGE and transferred to a nitrocellulose membrane using a Trans-Blot Turbo Transfer System apparatus according to the manufacturer's protocols (Bio-Rad). After incubation with 5% nonfat milk in TBST (10 mM Tris pH 8.0, 150 mM NaCl, 0.2% Tween 20) for 60 min, the membrane was washed three times with TBST and incubated with primary antibodies against t-FGFR2 (1:1,000; Cell Signaling Technology, Danvers, MA, USA, #23328), *p*-FGFR2 (1:1,000; Thermo Fisher Scientific, #PA5-64796), ERK1/2 (1:1,000; Cell Signaling Technology, #9102), *p*-ERK1/2 (1:1,000; Cell Signaling Technology, #9101), RUNX2 (1:1,000; Cell Signaling Technology; #12556) and GAPDH (1:1,000; Thermo Fisher Scientific) at 4°C for 12 h (O/N), followed by secondary peroxidase-conjugated antibodies (1:2,000). The chemiluminescent blots were imaged with the ChemiDoc MP imager (Bio-Rad). Densitometric analysis was carried out using the Band Analysis tools of ImageLab software version 6.0 (Bio-Rad) and relative bands intensity were normalized to GAPDH.

Statistical analysis

Data were analyzed using GraphPad Prism software version 10 (San Diego, CA, USA). The graphs were reported as means with standard deviation (SD) of the mean. Unpaired Student's t test was performed

for determining statistical differences between groups and probability values $p < 0.05$ were considered significant.

DATA AND CODE AVAILABILITY

The data related to this study are fully documented in the paper or in the Supplemental materials.

ACKNOWLEDGMENTS

This work was funded by AFM-Téléthon (Research Grant no. 23607 to W.L.), by POR FESR Lazio 2014–2020 (Protocol: A0375-2020- 36576 to W.L.), and by funds from Università Cattolica del Sacro Cuore to W.L. ("Linea D1 - 2021"). This study was also supported by the European Union - Next Generation EU within the MUR National Recovery and Resilience Plan (NRRP) - M4C2 - Action 1.4 - Call "Potenziamento strutture di ricerca e di campioni nazionali di R&S", Project CN3 "National Center for Gene Therapy and Drugs based on RNA Technology", no. CN00000041 [Spoke #6 "RNA Drug Development", CUP B83C22002860006 to P.C. The authors would like to acknowledge the Regenerative Medicine Research Center (CROME) of the Università Cattolica del Sacro Cuore. We thank Dr Diego Sibilia and Dr Domiziano Dario Tosi for their support in immunoblotting analyses. The authors are extremely grateful to the patients' families, who provided their consent to participate in the study.

AUTHOR CONTRIBUTIONS

Conceptualization: W.L., A.A., E.F., P.C., and O.P.; Methodology: F.T., L.D.P., and W.L.; Patients enrollment and specimen collection: G.T. and L.M.; Investigation: F.T., M.S., A.V., L.P., and G.T.; Data curation: F.T., L.P., and M.S.; Writing—original draft preparation: F.T., L.P, E.F., and P.C.; Writing—review and editing: W.L., A.A., P.C., and E.F.; Supervision: W.L. and E.F.; Technical support, M.S., A.V., and G.T.; Funding acquisition, W.L., P.C., and E.F. All authors have read and agreed to the published version of the manuscript.

DECLARATION OF INTERESTS

P.C. and E.F. are inventors on patent application EP3186192B1 held by Thena Biotech that covers fusion proteins based on human ferritins and methods of use thereof.

SUPPLEMENTAL INFORMATION

Supplemental information can be found online at https://doi.org/10.1016/j.omtn.2024.102427.

REFERENCES

1. Conrady, C.D., and Patel, B.C. (2024). Crouzon Syndrome. In StatPearls (StatPearls Publishing).
2. Katouni, K., Nikolaou, A., Mariolis, T., Protogerou, V., Chrysikos, D., Theofilopoulou, S., and Filippou, D. (2023). Syndromic Craniosynostosis: A Comprehensive Review. Cureus *15*, e50448. https://doi.org/10.7759/cureus.50448.
3. Lin, Y., Gao, H., Ai, S., Eswarakumar, J.V.P., Zhu, Y., Chen, C., Li, T., Liu, B., Jiang, H., Liu, Y., et al. (2017). FGFR2 mutations and associated clinical observations in two Chinese patients with Crouzon syndrome. Mol. Med. Rep. *16*, 5841–5846. https://doi.org/10.3892/mmr.2017.7397.
4. Al-Namnam, N.M., Hariri, F., Thong, M.K., and Rahman, Z.A. (2019). Crouzon syndrome: Genetic and intervention review. J. Oral Biol. Craniofac. Res. *9*, 37–39. https://doi.org/10.1016/j.jobcr.2018.08.007.
5. Kaur, H., Singh Waraich, H., and Sharma, C.M. (2006). Crouzon syndrome: A case report and review of literature. Indian J. Otolaryngol. Head Neck Surg. *58*, 381–382. https://doi.org/10.1007/BF03049602.
6. Reardon, W., Winter, R.M., Rutland, P., Pulleyn, L.J., Jones, B.M., and Malcolm, S. (1994). Mutations in the fibroblast growth factor receptor 2 gene cause Crouzon syndrome. Nat. Genet. *8*, 98–103. https://doi.org/10.1038/ng0994-98.
7. Ko, J.M. (2016). Genetic Syndromes Associated with Craniosynostosis. J. Korean Neurosurg. Soc. *59*, 187–191. https://doi.org/10.3340/jkns.2016.59.3.187.
8. Matsumoto, K., Urano, Y., Kubo, Y., Nakanishi, H., and Arase, S. (1998). Mutation of the fibroblast growth factor receptor 2 gene in Japanese patients with Apert syndrome. Plast. Reconstr. Surg. *101*, 307–311. https://doi.org/10.1097/00006534-199802000-00007.
9. Azoury, S.C., Reddy, S., Shukla, V., and Deng, C.X. (2017). Fibroblast Growth Factor Receptor 2 (FGFR2) Mutation Related Syndromic Craniosynostosis. Int. J. Biol. Sci. *13*, 1479–1488. https://doi.org/10.7150/ijbs.22373.
10. Su, N., Jin, M., and Chen, L. (2014). Role of FGF/FGFR signaling in skeletal development and homeostasis: learning from mouse models. Bone Res. *2*, 14003. https://doi.org/10.1038/boneres.2014.3.
11. Pfaff, M.J., Xue, K., Li, L., Horowitz, M.C., Steinbacher, D.M., and Eswarakumar, J.V.P. (2016). FGFR2c-mediated ERK-MAPK activity regulates coronal suture development. Dev. Biol. *415*, 242–250. https://doi.org/10.1016/j.ydbio.2016.03.026.
12. Twigg, S.R.F., and Wilkie, A.O.M. (2015). A Genetic-Pathophysiological Framework for Craniosynostosis. Am. J. Hum. Genet. *97*, 359–377. https://doi.org/10.1016/j.ajhg.2015.07.006.
13. Park, O.-J., Kim, H.-J., Woo, K.-M., Baek, J.-H., and Ryoo, H.-M. (2010). FGF2-activated ERK Mitogen-activated Protein Kinase Enhances Runx2 Acetylation and Stabilization. J. Biol. Chem. *285*, 3568–3574. https://doi.org/10.1074/jbc.M109.055053.
14. Bok, S., Yallowitz, A.R., Sun, J., McCormick, J., Cung, M., Hu, L., Lalani, S., Li, Z., Sosa, B.R., Baumgartner, T., et al. (2023). A multi-stem cell basis for craniosynostosis and calvarial mineralization. Nature *621*, 804–812. https://doi.org/10.1038/s41586-023-06526-2.
15. Di Pietro, L., Barba, M., Prampolini, C., Ceccariglia, S., Frassanito, P., Vita, A., Guadagni, E., Bonvissuto, D., Massimi, L., Tamburrini, G., et al. (2020). GLI1 and AXIN2 Are Distinctive Markers of Human Calvarial Mesenchymal Stromal Cells in Nonsyndromic Craniosynostosis. Int. J. Mol. Sci. *21*, 4356. https://doi.org/10.3390/ijms21124356.
16. Helman, S.N., Badhey, A., Kadakia, S., and Myers, E. (2014). Revisiting Crouzon syndrome: reviewing the background and management of a multifaceted disease. Oral Maxillofac. Surg. *18*, 373–379. https://doi.org/10.1007/s10006-014-0467-0.
17. Wilkie, A.O.M., Johnson, D., and Wall, S.A. (2017). Clinical Genetics of Craniosynostosis. Curr. Opin. Pediatr. *29*, 622–628. https://doi.org/10.1097/MOP.0000000000000542.
18. Mathijssen, I.M.J. (2015). Guideline for Care of Patients With the Diagnoses of Craniosynostosis: Working Group on Craniosynostosis. J. Craniofac. Surg. *26*, 1735–1807. https://doi.org/10.1097/SCS.0000000000002016.
19. Faasse, M., and Mathijssen, I.M.J.; ERN CRANIO Working Group on Craniosynostosis (2023). Guideline on Treatment and Management of Craniosynostosis: Patient and Family Version. J. Craniofac. Surg. *34*, 418–433. https://doi.org/10.1097/SCS.0000000000009143.
20. Bowling, E.L., and Burstein, F.D. (2006). Crouzon syndrome. Optometry *77*, 217–222. https://doi.org/10.1016/j.optm.2006.03.005.
21. Melville, H., Wang, Y., Taub, P.J., and Jabs, E.W. (2010). Genetic basis of potential therapeutic strategies for craniosynostosis. Am. J. Med. Genet. *152*, 3007–3015. https://doi.org/10.1002/ajmg.a.33703.
22. Utria, A.F., Mundinger, G.S., Bellamy, J.L., Zhou, J., Ghasemzadeh, A., Yang, R., Jallo, G.I., Ahn, E.S., and Dorafshar, A.H. (2015). The importance of timing in optimizing cranial vault remodeling in syndromic craniosynostosis. Plast. Reconstr. Surg. *135*, 1077–1084. https://doi.org/10.1097/PRS.0000000000001058.
23. Kyprianou, C., and Chatzigianni, A. (2018). Crouzon syndrome: A comprehensive review. Balkan J. Dent. Med. *22*, 1–6. https://doi.org/10.2478/bjdm-2018-0001.
24. Kajdic, N., Spazzapan, P., and Velnar, T. (2018). Craniosynostosis - Recognition, clinical characteristics, and treatment. Bosn. J. Basic Med. Sci. *18*, 110–116. https://doi.org/10.17305/bjbms.2017.2083.
25. Wu, S.-H., Liu, T.-J., Fan, S.-S., Chen, Z.-H., Wang, X.-L., and Gu, S. (2021). Severe chemosis and treatment following fronto-orbital advancement surgery for Crouzon syndrome. Medicine (Baltim.) *100*, e24693. https://doi.org/10.1097/MD.0000000000024693.
26. Hermann, C.D., Hyzy, S.L., Olivares-Navarrete, R., Walker, M., Williams, J.K., Boyan, B.D., and Schwartz, Z. (2016). Craniosynostosis and Resynostosis: Models, Imaging, and Dental Implications. J. Dent. Res. *95*, 846–852. https://doi.org/10.1177/0022034516643315.

27. Rachwalski, M., Khonsari, R.H., and Paternoster, G. (2019). Current Approaches in the Development of Molecular and Pharmacological Therapies in Craniosynostosis Utilizing Animal Models. Mol. Syndromol. *10*, 115–123. https://doi.org/10.1159/000493535.

28. McIntosh, I., Bellus, G.A., and Jab, E.W. (2000). The pleiotropic effects of fibroblast growth factor receptors in mammalian development. Cell Struct. Funct. *25*, 85–96. https://doi.org/10.1247/csf.25.85.

29. Shukla, V., Coumoul, X., Wang, R.-H., Kim, H.-S., and Deng, C.-X. (2007). RNA interference and inhibition of MEK-ERK signaling prevent abnormal skeletal phenotypes in a mouse model of craniosynostosis. Nat. Genet. *39*, 1145–1150. https://doi.org/10.1038/ng2096.

30. Luo, F., Xie, Y., Wang, Z., Huang, J., Tan, Q., Sun, X., Li, F., Li, C., Liu, M., Zhang, D., et al. (2018). Adeno-Associated Virus-Mediated RNAi against Mutant Alleles Attenuates Abnormal Calvarial Phenotypes in an Apert Syndrome Mouse Model. Mol. Ther. Nucleic Acids *13*, 291–302. https://doi.org/10.1016/j.omtn.2018.09.012.

31. Myo, A.C., Kobayashi, Y., Niki, Y., Kamimoto, H., and Moriyama, K. (2023). Exosome-mediated small interfering RNA delivery inhibits aberrant osteoblast differentiation in Apert syndrome model mice. Arch. Oral Biol. *153*, 105753. https://doi.org/10.1016/j.archoralbio.2023.105753.

32. Mitchell, M.J., Billingsley, M.M., Haley, R.M., Wechsler, M.E., Peppas, N.A., and Langer, R. (2021). Engineering precision nanoparticles for drug delivery. Nat. Rev. Drug Discov. *20*, 101–124. https://doi.org/10.1038/s41573-020-0090-8.

33. Mendes, B.B., Conniot, J., Avital, A., Yao, D., Jiang, X., Zhou, X., Sharf-Pauker, N., Xiao, Y., Adir, O., Liang, H., et al. (2022). Nanodelivery of nucleic acids. Nat. Rev. Methods Primers *2*, 24. https://doi.org/10.1038/s43586-022-00104-y.

34. Hamimed, S., Jabberi, M., and Chatti, A. (2022). Nanotechnology in drug and gene delivery. Naunyn-Schmiedeberg's Arch. Pharmacol. *395*, 769–787. https://doi.org/10.1007/s00210-022-02245-z.

35. Truffi, M., Fiandra, L., Sorrentino, L., Monieri, M., Corsi, F., and Mazzucchelli, S. (2016). Ferritin nanocages: A biological platform for drug delivery, imaging and theranostics in cancer. Pharmacol. Res. *107*, 57–65. https://doi.org/10.1016/j.phrs.2016.03.002.

36. Mosca, L., Falvo, E., Ceci, P., Poser, E., Genovese, I., Guarguaglini, G., and Colotti, G. (2017). Use of Ferritin-Based Metal-Encapsulated Nanocarriers as Anticancer Agents. Appl. Sci. *7*, 101. https://doi.org/10.3390/app7010101.

37. Zhu, Y., Zhu, Y., Cao, T., Liu, X., Liu, X., Yan, Y., Shi, Y., and Wang, J.-C. (2023). Ferritin-based nanomedicine for disease treatment. Med. Rev. *3*, 49–74. https://doi.org/10.1515/mr-2023-0001.

38. Pediconi, N., Ghirga, F., Del Plato, C., Peruzzi, G., Athanassopoulos, C.M., Mori, M., Crestoni, M.E., Corinti, D., Ugozzoli, F., Massera, C., et al. (2021). Design and Synthesis of Piperazine-Based Compounds Conjugated to Humanized Ferritin as Delivery System of siRNA in Cancer Cells. Bioconjug. Chem. *32*, 1105–1116. https://doi.org/10.1021/acs.bioconjchem.1c00137.

39. Marrocco, F., Falvo, E., Mosca, L., Tisci, G., Arcovito, A., Reccagni, A., Limatola, C., Bernardini, R., Ceci, P., D'Alessandro, G., and Colotti, G. (2024). Nose-to-brain selective drug delivery to glioma via ferritin-based nanovectors reduces tumor growth and improves survival rate. Cell Death Dis. *15*, 262. https://doi.org/10.1038/s41419-024-06653-2.

40. Fracasso, G., Falvo, E., Tisci, G., Sala, G., Colotti, G., Cingarlini, S., Tito, C., Bibbo, S., Frusteri, C., Tremante, E., et al. (2023). Widespread in vivo efficacy of The-0504: A conditionally-activatable nanoferritin for tumor-agnostic targeting of CD71-expressing cancers. Heliyon *9*, e20770. https://doi.org/10.1016/j.heliyon.2023.e20770.

41. Falvo, E., Malagrinò, F., Arcovito, A., Fazi, F., Colotti, G., Tremante, E., Di Micco, P., Braca, A., Opri, R., Giuffrè, A., et al. (2018). The presence of glutamate residues on the PAS sequence of the stimuli-sensitive nano-ferritin improves in vivo biodistribution and mitoxantrone encapsulation homogeneity. J. Control. Release *275*, 177–185. https://doi.org/10.1016/j.jconrel.2018.02.025.

42. He, J., Xu, S., and Mixson, A.J. (2020). The Multifaceted Histidine-Based Carriers for Nucleic Acid Delivery: Advances and Challenges. Pharmaceutics *12*, 774. https://doi.org/10.3390/pharmaceutics12080774.

43. López-Laguna, H., Cubarsi, R., Unzueta, U., Mangues, R., Vázquez, E., and Villaverde, A. (2020). Endosomal escape of protein nanoparticles engineered through humanized histidine-rich peptides. Sci. China Mater. *63*, 644–653. https://doi.org/10.1007/s40843-019-1231-y.

44. Chang, K.-L., Higuchi, Y., Kawakami, S., Yamashita, F., and Hashida, M. (2010). Efficient gene transfection by histidine-modified chitosan through enhancement of endosomal escape. Bioconjug. Chem. *21*, 1087–1095. https://doi.org/10.1021/bc1000609.

45. Shamsi, M.H., and Kraatz, H.-B. (2010). Probing nucleobase mismatch variations by electrochemical techniques: exploring the effects of position and nature of the single-nucleotide mismatch. Analyst *135*, 2280–2285. https://doi.org/10.1039/C0AN00184H.

46. Ahmed, F., and Raghava, G.P.S. (2011). Designing of highly effective complementary and mismatch siRNAs for silencing a gene. PLoS One *6*, e23443. https://doi.org/10.1371/journal.pone.0023443.

47. Huang, H., Qiao, R., Zhao, D., Zhang, T., Li, Y., Yi, F., Lai, F., Hong, J., Ding, X., Yang, Z., et al. (2009). Profiling of mismatch discrimination in RNAi enabled rational design of allele-specific siRNAs. Nucleic Acids Res. *37*, 7560–7569. https://doi.org/10.1093/nar/gkp835.

48. Zhu, S., Chen, W., Masson, A., and Li, Y.-P. (2024). Cell signaling and transcriptional regulation of osteoblast lineage commitment, differentiation, bone formation, and homeostasis. Cell Discov. *10*, 71. https://doi.org/10.1038/s41421-024-00689-6.

49. Komori, T. (2019). Regulation of Proliferation, Differentiation and Functions of Osteoblasts by Runx2. Int. J. Mol. Sci. *20*, 1694. https://doi.org/10.3390/ijms20071694.

50. Miraoui, H., Oudina, K., Petite, H., Tanimoto, Y., Moriyama, K., and Marie, P.J. (2009). Fibroblast Growth Factor Receptor 2 Promotes Osteogenic Differentiation in Mesenchymal Cells via ERK1/2 and Protein Kinase C Signaling. J. Biol. Chem. *284*, 4897–4904. https://doi.org/10.1074/jbc.M805432200.

51. Connolly, J.P., Gruss, J., Seto, M.L., Whelan, M.F., Ellenbogen, R., Weiss, A., Buchman, S.R., and Cunningham, M.L. (2004). Progressive postnatal craniosynostosis and increased intracranial pressure. Plast. Reconstr. Surg. *113*, 1313–1323. https://doi.org/10.1097/01.prs.0000111593.96440.30.

52. Geisler, E.L., Hallac, R.R., Perez, J.K., and Kane, A.A. (2021). Progressive Postnatal Pansynostosis in Crouzon Syndrome. J. Craniofac. Surg. *32*, e62–e64. https://doi.org/10.1097/SCS.0000000000006931.

53. Lee, H.Q., Hutson, J.M., Wray, A.C., Lo, P.A., Chong, D.K., Holmes, A.D., and Greensmith, A.L. (2012). Analysis of Morbidity and Mortality in Surgical Management of Craniosynostosis. J. Craniofac. Surg. *23*, 1256–1261. https://doi.org/10.1097/SCS.0b013e31824e26d6.

54. Yin, S., Wang, Y., Zhang, B., Qu, Y., Liu, Y., Dai, S., Zhang, Y., Wang, Y., and Bi, J. (2021). Engineered Human Heavy-Chain Ferritin with Half-Life Extension and Tumor Targeting by PAS and RGDK Peptide Functionalization. Pharmaceutics *13*, 521. https://doi.org/10.3390/pharmaceutics13040521.

55. Eswarakumar, V.P., Ozcan, F., Lew, E.D., Bae, J.H., Tomé, F., Booth, C.J., Adams, D.J., Lax, I., and Schlessinger, J. (2006). Attenuation of signaling pathways stimulated by pathologically activated FGF-receptor 2 mutants prevents craniosynostosis. Proc. Natl. Acad. Sci. USA *103*, 18603–18608. https://doi.org/10.1073/pnas.0609157103.

56. Perlyn, C.A., Morriss-Kay, G., Darvann, T., Tenenbaum, M., and Ornitz, D.M. (2006). A model for the pharmacological treatment of crouzon syndrome. Neurosurgery *59*, 210–215. , discussion 210-215. https://doi.org/10.1227/01.NEU.0000224323.53866.1E.

57. Wang, Y., Liu, Y., Chen, H., Liu, X., Zhang, Y., Wang, Y., and Gu, Y. (2022). FGFR2 Mutation p.Cys342Arg Enhances Mitochondrial Metabolism-Mediated Osteogenesis via FGF/FGFR-AMPK-Erk1/2 Axis in Crouzon Syndrome. Cells *11*, 3129. https://doi.org/10.3390/cells11193129.

58. Wang, Y., Zhou, X., Oberoi, K., Phelps, R., Couwenhoven, R., Sun, M., Rezza, A., Holmes, G., Percival, C.J., Friedenthal, J., et al. (2012). p38 Inhibition ameliorates skin and skull abnormalities in Fgfr2 Beare-Stevenson mice. J. Clin. Invest. *122*, 2153–2164. https://doi.org/10.1172/JCI62644.

59. Balek, L., Gudernova, I., Vesela, I., Hampl, M., Oralova, V., Kunova Bosakova, M., Varecha, M., Nemec, P., Hall, T., Abbadessa, G., et al. (2017). ARQ 087 inhibits FGFR signaling and rescues aberrant cell proliferation and differentiation in experimental models of craniosynostoses and chondrodysplasias caused by activating

mutations in FGFR1, FGFR2 and FGFR3. Bone *105*, 57–66. https://doi.org/10.1016/j.bone.2017.08.016.

60. Shen, K., Krakora, S.M., Cunningham, M., Singh, M., Wang, X., Hu, F.Z., Post, J.C., and Ehrlich, G.D. (2009). Medical treatment of craniosynostosis: recombinant Noggin inhibits coronal suture closure in the rat craniosynostosis model. Orthod. Craniofac. Res. *12*, 254–262. https://doi.org/10.1111/j.1601-6343.2009.01460.x.

61. Xu, W., Luo, F., Wang, Q., Tan, Q., Huang, J., Zhou, S., Wang, Z., Sun, X., Kuang, L., Jin, M., et al. (2017). Inducible Activation of FGFR2 in Adult Mice Promotes Bone Formation After Bone Marrow Ablation. J. Bone Miner. Res. *32*, 2194–2206. https://doi.org/10.1002/jbmr.3204.

62. Chen, P., Zhang, L., Weng, T., Zhang, S., Sun, S., Chang, M., Li, Y., Zhang, B., and Zhang, L. (2014). A Ser252Trp mutation in fibroblast growth factor receptor 2 (FGFR2) mimicking human Apert syndrome reveals an essential role for FGF signaling in the regulation of endochondral bone formation. PLoS One *9*, e87311. https://doi.org/10.1371/journal.pone.0087311.

63. Greenwald, J.A., Mehrara, B.J., Spector, J.A., Warren, S.M., Fagenholz, P.J., Smith, L.E., Bouletreau, P.J., Crisera, F.E., Ueno, H., and Longaker, M.T. (2001). In vivo modulation of FGF biological activity alters cranial suture fate. Am. J. Pathol. *158*, 441–452. https://doi.org/10.1016/s0002-9440(10)63987-9.

64. McDowell, L.M., Frazier, B.A., Studelska, D.R., Giljum, K., Chen, J., Liu, J., Yu, K., Ornitz, D.M., and Zhang, L. (2006). Inhibition or activation of Apert syndrome FGFR2 (S252W) signaling by specific glycosaminoglycans. J. Biol. Chem. *281*, 6924–6930. https://doi.org/10.1074/jbc.M512932200.

65. Warren, S.M., Proctor, M.R., Bartlett, S.P., Blount, J.P., Buchman, S.R., Burnett, W., Fearon, J.A., Keating, R., Muraszko, K.M., Rogers, G.F., et al. (2012). Parameters of care for craniosynostosis: craniofacial and neurologic surgery perspectives. Plast. Reconstr. Surg. *129*, 731–737. https://doi.org/10.1097/PRS.0b013e3182412a50.

66. Tanimoto, Y., Yokozeki, M., Hiura, K., Matsumoto, K., Nakanishi, H., Matsumoto, T., Marie, P.J., and Moriyama, K. (2004). A soluble form of fibroblast growth factor receptor 2 (FGFR2) with S252W mutation acts as an efficient inhibitor for the enhanced osteoblastic differentiation caused by FGFR2 activation in Apert syndrome. J. Biol. Chem. *279*, 45926–45934. https://doi.org/10.1074/jbc.M404824200.

67. Yokota, M., Kobayashi, Y., Morita, J., Suzuki, H., Hashimoto, Y., Sasaki, Y., Akiyoshi, K., and Moriyama, K. (2014). Therapeutic Effect of Nanogel-Based Delivery of Soluble FGFR2 with S252W Mutation on Craniosynostosis. PLoS One *9*, e101693. https://doi.org/10.1371/journal.pone.0101693.

68. Lees-Shepard, J.B., Stoessel, S.J., Chandler, J.T., Bouchard, K., Bento, P., Apuzzo, L.N., Devarakonda, P.M., Hunter, J.W., and Goldhamer, D.J. (2022). An anti-ACVR1 antibody exacerbates heterotopic ossification by fibro-adipogenic progenitors in fibrodysplasia ossificans progressiva mice. J. Clin. Invest. *132*, e153795. https://doi.org/10.1172/JCI153795.

69. Trochet, D., Prudhon, B., Vassilopoulos, S., and Bitoun, M. (2015). Therapy for dominant inherited diseases by allele-specific RNA interference: successes and pitfalls. Curr. Gene Ther. *15*, 503–510. https://doi.org/10.2174/1566523215666150812115730.

70. Fernandes, M.B.L., Maximino, L.P., Perosa, G.B., Abramides, D.V.M., Passos-Bueno, M.R., and Yacubian-Fernandes, A. (2016). Apert and Crouzon syndromes-Cognitive development, brain abnormalities, and molecular aspects. Am. J. Med. Genet. *170*, 1532–1537. https://doi.org/10.1002/ajmg.a.37640.

71. Jabs, E.W., Li, X., Scott, A.F., Meyers, G., Chen, W., Eccles, M., Mao, J.I., Charnas, L.R., Jackson, C.E., and Jaye, M. (1994). Jackson-Weiss and Crouzon syndromes are allelic with mutations in fibroblast growth factor receptor 2. Nat. Genet. *8*, 275–279. https://doi.org/10.1038/ng1194-275.

72. Grover, S.B., Bhayana, A., Grover, H., Kapoor, S., and Chellani, H. (2019). Imaging diagnosis of Crouzon syndrome in two cases confirmed on genetic studies - with a brief review. Indian J. Radiol. Imaging *29*, 442–447. https://doi.org/10.4103/ijri.IJRI_353_19.

73. Robertson, S.C., Meyer, A.N., Hart, K.C., Galvin, B.D., Webster, M.K., and Donoghue, D.J. (1998). Activating mutations in the extracellular domain of the fibroblast growth factor receptor 2 function by disruption of the disulfide bond in the third immunoglobulin-like domain. Proc. Natl. Acad. Sci. USA *95*, 4567–4572.

74. Kress, W., Collmann, H., Büsse, M., Halliger-Keller, B., and Mueller, C.R. (2000). Clustering of FGFR2 gene mutations inpatients with Pfeiffer and Crouzon syndromes (FGFR2-associated craniosynostoses). Cytogenet. Cell Genet. *91*, 134–137. https://doi.org/10.1159/000056833.

75. Steinberger, D., Vriend, G., Mulliken, J.B., and Müller, U. (1998). The mutations in FGFR2-associated craniosynostoses are clustered in five structural elements of immunoglobulin-like domain III of the receptor. Hum. Genet. *102*, 145–150. https://doi.org/10.1007/s004390050668.

76. Kim, D.-H., Behlke, M.A., Rose, S.D., Chang, M.-S., Choi, S., and Rossi, J.J. (2005). Synthetic dsRNA Dicer substrates enhance RNAi potency and efficacy. Nat. Biotechnol. *23*, 222–226. https://doi.org/10.1038/nbt1051.

77. Rose, S.D., Kim, D.-H., Amarzguioui, M., Heidel, J.D., Collingwood, M.A., Davis, M.E., Rossi, J.J., and Behlke, M.A. (2005). Functional polarity is introduced by Dicer processing of short substrate RNAs. Nucleic Acids Res. *33*, 4140–4156. https://doi.org/10.1093/nar/gki732.

78. Zhou, J., Song, M.-S., Jacobi, A.M., Behlke, M.A., Wu, X., and Rossi, J.J. (2012). Deep Sequencing Analyses of DsiRNAs Reveal the Influence of 3' Terminal Overhangs on Dicing Polarity, Strand Selectivity, and RNA Editing of siRNAs. Mol. Ther. Nucleic Acids *1*, e17. https://doi.org/10.1038/mtna.2012.6.

79. Haley, B., and Zamore, P.D. (2004). Kinetic analysis of the RNAi enzyme complex. Nat. Struct. Mol. Biol. *11*, 599–606. https://doi.org/10.1038/nsmb780.

80. Schwarz, D.S., Ding, H., Kennington, L., Moore, J.T., Schelter, J., Burchard, J., Linsley, P.S., Aronin, N., Xu, Z., and Zamore, P.D. (2006). Designing siRNA That Distinguish between Genes That Differ by a Single Nucleotide. PLoS Genet. *2*, e140. https://doi.org/10.1371/journal.pgen.0020140.

81. Xie, Y., Su, N., Yang, J., Tan, Q., Huang, S., Jin, M., Ni, Z., Zhang, B., Zhang, D., Luo, F., et al. (2020). FGF/FGFR signaling in health and disease. Signal Transduct. Target. Ther. *5*, 181. https://doi.org/10.1038/s41392-020-00222-7.

82. Ornitz, D.M., and Marie, P.J. (2015). Fibroblast growth factor signaling in skeletal development and disease. Genes Dev. *29*, 1463–1486. https://doi.org/10.1101/gad.266551.115.

83. Hojo, H. (2023). Emerging RUNX2-Mediated Gene Regulatory Mechanisms Consisting of Multi-Layered Regulatory Networks in Skeletal Development. Int. J. Mol. Sci. *24*, 2979. https://doi.org/10.3390/ijms24032979.

84. Komori, T. (2022). Whole Aspect of Runx2 Functions in Skeletal Development. Int. J. Mol. Sci. *23*, 5776. https://doi.org/10.3390/ijms23105776.

85. Yuan, G., Lin, X., Liu, Y., Greenblatt, M.B., and Xu, R. (2024). Skeletal stem cells in bone development, homeostasis and disease. Protein Cell *15*, 559–574. https://doi.org/10.1093/procel/pwae008.

86. Debnath, S., Yallowitz, A.R., McCormick, J., Lalani, S., Zhang, T., Xu, R., Li, N., Liu, Y., Yang, Y.S., Eiseman, M., et al. (2018). Discovery of a periosteal stem cell mediating intramembranous bone formation. Nature *562*, 133–139. https://doi.org/10.1038/s41586-018-0554-8.

87. Raval, N., Jogi, H., Gondaliya, P., Kalia, K., and Tekade, R.K. (2019). Method and its Composition for encapsulation, stabilization, and delivery of siRNA in Anionic polymeric nanoplex: An In vitro- In vivo Assessment. Sci. Rep. *9*, 16047. https://doi.org/10.1038/s41598-019-52390-4.

88. Alshaer, W., Zureigat, H., Al Karaki, A., Al-Kadash, A., Gharaibeh, L., Hatmal, M.M., Aljabali, A.A.A., and Awidi, A. (2022). Corrigendum to "siRNA: Mechanism of action, challenges, and therapeutic approaches" [Eur. J. Pharmacol. 905 (2021) 174178]. Eur. J. Pharmacol. *916*, 174741. https://doi.org/10.1016/j.ejphar.2022.174741.

89. Sajid, M.I., Moazzam, M., Kato, S., Yeseom Cho, K., and Tiwari, R.K. (2020). Overcoming Barriers for siRNA Therapeutics: From Bench to Bedside. Pharm. Basel Switz. *13*, 294. https://doi.org/10.3390/ph13100294.

90. Montemiglio, L.C., Testi, C., Ceci, P., Falvo, E., Pitea, M., Savino, C., Arcovito, A., Peruzzi, G., Baiocco, P., Mancia, F., et al. (2019). Cryo-EM structure of the human ferritin-transferrin receptor 1 complex. Nat. Commun. *10*, 1121. https://doi.org/10.1038/s41467-019-09098-w.

91. Fracasso, G., Falvo, E., Colotti, G., Fazi, F., Ingegnere, T., Amalfitano, A., Doglietto, G.B., Alfieri, S., Boffi, A., Morea, V., et al. (2016). Selective delivery of doxorubicin by novel stimuli-sensitive nano-ferritins overcomes tumor refractoriness. J. Control. Release *239*, 10–18. https://doi.org/10.1016/j.jconrel.2016.08.010.

92. Page-McCaw, A., Ewald, A.J., and Werb, Z. (2007). Matrix metalloproteinases and the regulation of tissue remodelling. Nat. Rev. Mol. Cell Biol. *8*, 221–233. https://doi.org/10.1038/nrm2125.

93. Meng, Z., Luan, L., Kang, Z., Feng, S., Meng, Q., and Liu, K. (2017). Histidine-enriched multifunctional peptide vectors with enhanced cellular uptake and endosomal escape for gene delivery. J. Mater. Chem. B *5*, 74–84. https://doi.org/10.1039/C6TB02862D.

94. Hooshmand, S.E., Jahanpeimay Sabet, M., Hasanzadeh, A., Kamrani Mousavi, S.M., Haeri Moghaddam, N., Hooshmand, S.A., Rabiee, N., Liu, Y., Hamblin, M.R., and Karimi, M. (2022). Histidine-enhanced gene delivery systems: The state of the art. J. Gene Med. *24*, e3415. https://doi.org/10.1002/jgm.3415.

95. Li, L., Muñoz-Culla, M., Carmona, U., Lopez, M.P., Yang, F., Trigueros, C., Otaegui, D., Zhang, L., and Knez, M. (2016). Ferritin-mediated siRNA delivery and gene silencing in human tumor and primary cells. Biomaterials *98*, 143–151. https://doi.org/10.1016/j.biomaterials.2016.05.006.

96. Elmén, J., Thonberg, H., Ljungberg, K., Frieden, M., Westergaard, M., Xu, Y., Wahren, B., Liang, Z., Ørum, H., Koch, T., and Wahlestedt, C. (2005). Locked nucleic acid (LNA) mediated improvements in siRNA stability and functionality. Nucleic Acids Res. *33*, 439–447. https://doi.org/10.1093/nar/gki193.

97. Lattanzi, W., Barba, M., Novegno, F., Massimi, L., Tesori, V., Tamburrini, G., Galgano, S., Bernardini, C., Caldarelli, M., Michetti, F., and Di Rocco, C. (2013). Lim mineralization protein is involved in the premature calvarial ossification in sporadic craniosynostoses. Bone *52*, 474–484. https://doi.org/10.1016/j.bone.2012.09.004.

98. Barba, M., Di Pietro, L., Massimi, L., Geloso, M.C., Frassanito, P., Caldarelli, M., Michetti, F., Della Longa, S., Romitti, P.A., Di Rocco, C., et al. (2019). Corrigendum to "BBS9 gene in nonsyndromic craniosynostosis: Role of the primary cilium in the aberrant ossification of the suture osteogenic niche" [Bone 112 (July 2018) 58-70]. Bone *121*, 293. https://doi.org/10.1016/j.bone.2019.02.004.

99. Palmieri, V., Barba, M., Di Pietro, L., Conti, C., De Spirito, M., Lattanzi, W., and Papi, M. (2018). Graphene Oxide Induced Osteogenesis Quantification by In-Situ 2D-Fluorescence Spectroscopy. Int. J. Mol. Sci. *19*, 3336. https://doi.org/10.3390/ijms19113336.

100. Falvo, E., Tremante, E., Fraioli, R., Leonetti, C., Zamparelli, C., Boffi, A., Morea, V., Ceci, P., and Giacomini, P. (2013). Antibody-drug conjugates: targeting melanoma with cisplatin encapsulated in protein-cage nanoparticles based on human ferritin. Nanoscale *5*, 12278–12285. https://doi.org/10.1039/c3nr04268e.